https://doi.org/10.5194/egusphere-2026-3239
Preprint. Discussion started: 18 June 2026

The radiative effect and climate responses of present-day wildfire emissions

Rafaila-Nikola Mourgela [1,2], Iulian-Alin Rosu [1,2], and Apostolos Voulgarakis [1,2]

[1]Laboratory of Atmospheric Environment and Climate Change, School of Chemical and Environmental Engineering, Technical University of Crete, Chania, 73100, Greece,

[2]Leverhulme Centre for Wildfires Environment and Society, Imperial College London, London, SW7 2AZ, UK

Correspondence to: Rafaila-Nikola Mourgela (rmourgela@tuc.gr)

Abstract. Aerosols exert spatially inhomogeneous radiative effects (REs) that can drastically perturb global and regional climate. While studies have investigated the impacts of regional anthropogenic aerosol emissions on climate, there is no past work systematically exploring the impacts of regional wildfire emissions. This study investigates the interconnection between wildfires and the atmosphere, focusing on the global RE and climate responses from wildfire emissions. We examine the effects of carbonaceous aerosols and O_3 precursors via atmosphere-only and ocean-atmosphere coupled simulations using EC-Earth3, driven by the CMIP6 wildfire emissions. Additional atmosphere-only perturbation simulations with wildfire emissions removed from selected regions, i.e., Boreal North America, South America, Africa, Boreal & Central Asia, and Equatorial Asia, were also performed to determine their local and remote effects. We identify which regions experience stronger RE and separate direct influences of emissions on radiation from secondary mechanisms. Our simulations indicate that the global RE of short-lived wildfire emissions is negative (cooling), dominated by aerosol-cloud interactions, with aerosol-radiation interactions and side effects via O_3, water vapor and surface albedo being particularly important in specific regions. The slow, ocean-mediated response dominates the total climate response to wildfire emissions, showing substantial global cooling, and pronounced regional effects on precipitation especially in the tropics. Wildfire emissions affect regions both locally and remotely to the emissions, as they alter circulation, land-atmosphere coupling, convection, and energy transport across the globe, producing a highly interconnected climate response. Overall, this study demonstrates that short-lived wildfire emissions can be a substantial modifier of the global climate system.

1 Introduction

Understanding the climate responses to wildfire emissions is of major importance as it benefits the current wildfire modelling and future projections (He et al., 2024). Wildfires are a key source of aerosols and trace gases, significantly affecting the Earth's radiative balance and consequently the climate system (Jiang et al., 2020; Voulgarakis and Field, 2015). For instance, The wildfire-emitted trace gases can interfere with radiation both directly, due to the emission of greenhouse gases, and

https://doi.org/10.5194/egusphere-2026-3239
Preprint. Discussion started: 18 June 2026

indirectly, due to the emission of ozone (O_3) precursors (Rowlinson et al., 2020; Voulgarakis and Field, 2015; Ward et al., 2012). The wildfire-emitted aerosols can directly interfere with radiation via scattering and absorption (direct aerosol effects, the so-called aerosol-radiation interactions (ARI)), and can affect cloud formation and their characteristics via microphysical and thermodynamic processes (indirect and semi-direct aerosol effects, the so-called aerosol-cloud interactions (ACI)) (Barjeste Vaezi et al., 2025; Jiang et al., 2016, 2020; Kalisoras et al., 2024; Li et al., 2022b; Myhre et al., 2013; Voulgarakis and Field, 2015). Specifically, absorbing aerosols, such as the wildfire-emitted black carbon (BC), cause localized warming, reducing relative humidity and eventually cloud cover (semi-direct effect) (Barjeste Vaezi et al., 2025; Li et al., 2022b). Moreover, the wildfire-emitted aerosols act as Cloud Condensation Nuclei (CCN) and ice-nucleating particles (INPs), fundamentally altering the microphysical properties of clouds (Barjeste Vaezi et al., 2025; Li et al., 2022b). The first indirect effect of aerosols on clouds is the Twomey Effect, according to which the smoke-laden cloud will have a higher concentration of smaller droplets compared to a "clean" cloud (Twomey, 1977). These numerous and smaller droplets increase the surface albedo of clouds, making them brighter and more reflective. The second indirect effect is the Albrecht Effect; the smaller droplets are less likely to collide and grow enough to precipitate, consequently increasing cloud lifetime and cloud thickness (Albrecht, 1989). Hence, the indirect effects of aerosols result on more persistent and reflective clouds, increasing the reflection of incoming radiation, while in contrast, the semi-direct effect results in cloud inhibition and potentially increasing the radiation that reaches the Earth's surface.

To quantify the influence of a perturbation, such as wildfire emissions, on Earth's radiative balance we use the term of radiative effect (RE) which is expressed in W/m² and can be positive or negative depending on whether the perturbation has a warming or a cooling effect respectively (Jiang et al., 2020). Globally, wildfire-emitted aerosols have been reported to exert a negative RE at the top of the atmosphere (TOA), approximately ranging between -1.6 W/m² and -0.4 W/m², and mainly driven by ACI (Clark et al., 2015; Grandey et al., 2016; Jiang et al., 2016, 2020; Landry et al., 2017; Tian et al., 2022; Ward et al., 2012; Zou et al., 2020). RE from ACI has been reported to range from approximately -1.6 W/m² to -0.2 W/m², while the RE from ARI has been reported to have greater variability, ranging from about -0.2 W/m² to +0.3 W/m² (Clark et al., 2015; Grandey et al., 2016; Jiang et al., 2016, 2020; Landry et al., 2017; Tian et al., 2022; Ward et al., 2012; Zou et al., 2020). In addition, the secondarily produced tropospheric O_3 has been reported to exert a positive RE, though small on a global scale (Chan et al., 2001; Natarajan et al., 2012; Ward et al., 2012). However, for both aerosols and O_3 the regional effects can be one to two orders of magnitude larger than the global mean (Chan et al., 2001; Chang et al., 2021; Jiang et al., 2016, 2020; Natarajan et al., 2012; Roșu et al., 2025; Thornhill et al., 2018; Tosca et al., 2013; Vescovini et al., 2024).

Wildfires also affect the surface albedo in both direct and indirect ways; directly via changing the landscapes and indirectly via the effects on climate/meteorology (and therefore snow/ice - further discussed below) and aerosol deposition. For instance, wildfire-emitted BC can increase surface albedo by depositing on snow- and ice-covered land surfaces, eventually darkening them and promoting snow and ice melting (Barjeste Vaezi et al., 2025; Li et al., 2022b; Tian et al., 2022; Ward et al., 2012). Previous studies have estimated the radiative effect due to aerosol-induced changes in surface albedo and found the global means ranging from -0.1 to 0.2 (Grandey et al., 2016; Jiang et al., 2016, 2020; Tian et al., 2022; Yan et al., 2021; Zou et al.,

https://doi.org/10.5194/egusphere-2026-3239
Preprint. Discussion started: 18 June 2026

2020). On the other hand, studies report the radiative effect of the direct changes in landscape due to wildfire between -0.2 W/m² and -0.03 W/m² on a global scale (López-Saldaña et al., 2015; Ward et al., 2012).

As a consequence of the radiative impacts, wildfire emissions also have large-scale meteorological impacts, which highlight the complexity of decoding wildfire effects on climate (Barjeste Vaezi et al., 2025; Jain et al., 2024; Roșu et al., 2025, 2026; Shawki et al., 2018; Stocker et al., 2021; Voulgarakis et al., 2015; Ward et al., 2012; Wells et al., 2023; van der Werf et al., 2010). Wildfire-emitted absorbing aerosols can warm and stabilize the lower atmosphere, suppress convection and cloud formation, and eventually reduce precipitation. In addition, the effects on atmospheric stability affect atmospheric circulation Wildfire-emitted aerosols can shift temperature gradients and modify regional and even large-scale circulation patterns (Barjeste Vaezi et al., 2025). On large scales, wildfires can affect the Hadley circulation, the Walker circulation, the El Niño Southern Oscillation (ENSO) and the inter-tropical convergence zone (ITCZ) with significant implications for drought and extreme events on a global scale (Barjeste Vaezi et al., 2025; Tosca et al., 2013). Overall, studies have found that wildfire aerosols mainly cause surface cooling, with global means ranging from -0.8 to -0.01 °C, and precipitation suppression, with global means ranging from −0.07 to −0.0006 mm/day (Grandey et al., 2016; Jiang et al., 2016, 2020; Landry et al., 2017; Li, 2020; Thornhill et al., 2018; Tian et al., 2022; Tosca et al., 2013; Xu et al., 2021).

The current study aims to quantify the role of wildfire emissions in the climate system. We have performed atmosphere-only and fully coupled ocean-atmosphere simulations to estimate the radiative and climate effects of present-day wildfire emissions using EC-Earth3 and the CMIP6 wildfire emissions dataset. The CMIP6 dataset is widely used and largely based on the Global Fire Emissions Database Version 4s (GFED4s), which relies on satellite observations (Feng et al., 2020). Given that the GFED4s is a well-established and extensively applied dataset, the CMIP6 wildfire emissions dataset serves as a community benchmark and is therefore deemed as the most suitable for the purposes of this study (Pan et al., 2020; Parrington et al., 2025). We focus on simulations with repeated conditions as our aim is to quantify the RE and the climate effects in equilibrium at present-day as it is typically done in such studies (Collins et al., 2017; Kramer et al., 2026; Liu et al., 2018; Myhre et al., 2017; Pincus et al., 2016; Samset et al., 2016). Therefore, the climatological emissions are repeated in the present work rather than interannually varying. Also, we performed five more atmosphere-only perturbation simulations with wildfire emissions removed from selected regions, i.e., Boreal North America, South America, Africa, Boreal & Central Asia, and Equatorial Asia, to determine the local and remote effects of regional wildfire emissions. We identify which regions experience stronger forcing from these emissions and separate the roles of different mechanisms in driving the radiative and climate impacts.

2 Methodology

2.1 Model and experimental design

Atmosphere-only (pdClim-type) and fully coupled ocean-atmosphere simulations were performed using the EC-Earth Earth System Model (ESM), and specifically the EC-Earth3-AerChem configuration (Döscher et al., 2022; van Noije et al., 2021).

https://doi.org/10.5194/egusphere-2026-3239
Preprint. Discussion started: 18 June 2026

The EC-Earth3-AerChem configuration incorporates interactive aerosols and atmospheric chemistry following the specifications of the Aerosol and Chemistry Model Intercomparison Project (AerChemMIP) (Collins et al., 2017; Döscher et al., 2022; van Noije et al., 2021). For the atmosphere-only set up, the IFS general circulation model (GCM) cycle 36r4 (Integrated Forecasting System), including the land surface module HTESSEL (Hydrology Tiled ECMWF Scheme of Surface Exchanges over Land), from the European Centre for Medium-Range Weather Forecasts (ECMWF) was coupled with the TM5 chemistry-transport model (CTM) (Tracer Model version 5). The IFS was used in its standard configuration (T255L91), featuring a horizontal resolution of approximately 80 km and 91 hybrid sigma-pressure levels in the vertical. TM5, on the other hand, was run with a horizontal resolution of 3° × 2° (longitude × latitude) and 34 hybrid sigma-pressure layers, with the uppermost layer extending to about 0.1 hPa. For the ocean-atmosphere set up, the atmospheric components (IFS, HTESSEL, and TM5) are coupled with the NEMO3.6 (Nucleus for European Modelling of the Ocean) ocean model and the LIM3 (Louvain-la-Neuve Sea Ice Model) sea-ice model. NEMO3.6 and LIM3 utilize the ORCA1 tripolar grid, providing a horizontal resolution of approximately 1° with 75 vertical layers. The IFS (T255L91) and TM5 (3°×2°) resolutions remain consistent with the atmosphere-only setup previously described. It is noted that the AerChem model configuration has been selected, in order to focus on the atmospheric impacts of fire emissions that control the corresponding radiative effects, as it's typically done in such studies (Collins et al., 2017; Kramer et al., 2026; Liu et al., 2018; Myhre et al., 2017; Samset et al., 2016).

A (31-year atmosphere-only) 100-year ocean-coupled control simulation was conducted without including wildfire emissions. This simulation was then repeated with wildfire emissions set to their 2015 levels according to the CMIP6 dataset and the SSP3-7.0 scenario (Feng et al., 2020). Note that in CMIP6, the year 2015 is effectively treated as a transition year from historical to future scenarios, therefore the 2015 emissions are almost identical in all SSPs as the scenarios are harmonized near 2015 in order to branch smoothly from the historical period (Turnock et al., 2020). Moreover, by design, the CMIP6 dataset does not aim to represent specific years in the emissions provided (e.g., the strongly anomalous wildfire emissions of 2015 due to El Niño conditions), but merely the average emissions of the period centered around a given year, i.e., in this case, the 2015 wildfire emissions represent the 10-year mean of 2005-2014. In all simulations, the (sea surface temperatures (SSTs), sea ice concentrations (SICs),) vegetation types and vegetation coverage, CH_4 and CO_2 mixing ratios, and all other forcings described by Döscher et al. (2022) were fixed at their 2015 levels (SSP3-7.0 scenario). Therefore, in the present configuration, evapotranspiration responds to changes in meteorological conditions and not to changes in vegetation properties. Anthropogenic emissions were prescribed at their 2015 levels based on the Community Emissions Data System (CEDS) dataset (Feng et al., 2020). Natural emissions were prescribed and calculated following the methodology described by van Noije et al. (2014, 2021). The first (1 year of the atmosphere-only) 50 years of the ocean-atmosphere simulations (was) were discarded as model spin-up time.

Five more perturbation atmosphere-only simulations were performed with wildfire emissions removed from selected regions, i.e., Boreal North America (hereafter BNA), South America (SA), Africa (AF), Boreal & Central Asia (BSA), and Equatorial Asia (EQ), to determine the effect of emissions from key wildfire activity regions, on a global scale. Figure 1 depicts the geographical boundaries adopted from the aforementioned regions in this study.

https://doi.org/10.5194/egusphere-2026-3239
Preprint. Discussion started: 18 June 2026

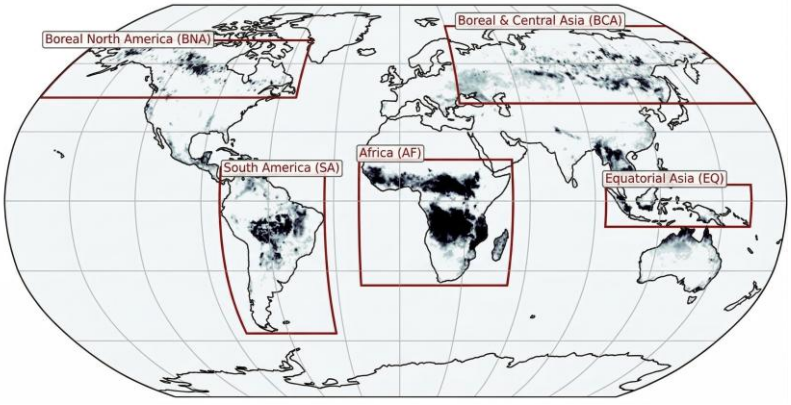

Figure 1: The geographical boundaries adopted in the present work for the perturbation atmosphere-only simulations with removed wildfire emissions from the selected regions. The shaded regions indicate the spatial distribution of the wildfire emissions according to the CMIP6 dataset and the SSP3-7.0 scenario for 2015 (Feng et al., 2020).

In terms of model evaluation, Gliß et al., (2021) compared the aerosol optical variables derived from different models against surface in situ, and ground- and space-based observations and found that TM5 and EC-Earth3 performed better than the rest of the examined models, having the lower biases. Moreover, EC-Earth3 generally demonstrates good skill in reproducing observed large-scale temperature and precipitation patterns with performance comparable to or exceeding that of many CMIP6 models (Bilbao et al., 2021; Chaudhary et al., 2025; Döscher et al., 2022; Liu et al., 2023; van Noije et al., 2021; Tang et al., 2021; Zhu et al., 2024). Evaluation against reanalysis datasets, such as ERA5, and observational datasets, such as GISTEMP, indicates that EC-Earth3 captures the global mean near-surface air temperature reasonably well, although it exhibits a warm global bias of approximately 0.5 K, primarily associated with a pronounced warm bias over the Southern Ocean and Antarctica (Döscher et al., 2022; van Noije et al., 2021). This bias, which is common among coupled climate models, has been largely attributed to deficiencies in the representation of shortwave cloud radiative effects (Döscher et al., 2022; Thomas et al., 2024). Furthermore, EC-Earth3 reproduces the global distribution of precipitation well, although it retains the well-known double Intertropical Convergence Zone (ITCZ) bias and tends to overestimate precipitation in the tropics, particularly in the Southern Hemisphere, partly as a consequence of the Southern Ocean warm bias and the associated strengthening of the hydrological cycle (Döscher et al., 2022). Nevertheless, several regional studies evaluate the precipitation derived from EC-Earth3 against reanalysis and observational datasets and highlight its strong performance in reproducing precipitation (Chaudhary et al., 2025; Liu et al., 2023; Roșu et al., 2026; Tang et al., 2021; Zhu et al., 2024). The model has been identified among the best-performing CMIP6 models for precipitation simulation over Southeast Asia, successfully reproduces observed precipitation–temperature relationships during the Indian Summer Monsoon, and accurately captures both the spatial patterns and interannual variability of extreme precipitation indices over South China and Indochina (Chaudhary et al., 2025; Liu et al., 2023; Roșu et al., 2026; Tang et al., 2021). Furthermore, EC-Earth3 has been shown to realistically represent the spatial and temporal characteristics

https://doi.org/10.5194/egusphere-2026-3239
Preprint. Discussion started: 18 June 2026

of compound wind–precipitation extremes (Zhu et al., 2024). Overall, while systematic biases in temperature and precipitation remain, particularly over the Southern Ocean and tropical precipitation belts, the available evidence suggests that EC-Earth3 provides a robust representation of temperature and precipitation.

2.2 Radiative Effect (RE) decomposition

In this work we are adopting the radiative forcing/effect decomposition proposed by Ghan (2013). Specifically, the decomposition of RE is considered as follows (Eq. 1):

$$RE = RE_{ARI} + RE_{ACI} + RE_{res} \quad (1)$$

- Aerosol-Radiation Interactions (RE_{ARI}): This component includes the aerosol direct radiative effect together with the semi-direct effect (from the perspective of aerosol-induced absorption) (Bellouin et al., 2020a; Ghan, 2013; Jiang et al., 2020; Kalisoras et al., 2024; Zelinka et al., 2014, 2023). The RE_{ARI} term is calculated as (Eq. 2):

  $$RE_{ARI} = \Delta(F - F_{af}) \quad (2)$$

  where F is the net radiative flux at the top-of-the-atmosphere (TOA), F_{af} is the corresponding flux calculated ignoring the scattering and absorption by aerosols, despite their presence in the atmosphere (i.e., aerosol-free forcing), and Δ denotes the difference between the perturbation and the control experiment.

- Aerosol-Cloud Interactions (RE_{ACI})**:** This component includes the effects on both cloud albedo and cloud persistence, such as the Twomey and the Albrecht effects, and the semi-direct effect, with the latter representing the effects on clouds associated with the aerosol-induced absorption and atmospheric heating (Bellouin et al., 2020a; Ghan, 2013; Jiang et al., 2020; Kalisoras et al., 2024; Zelinka et al., 2014, 2023). The RE_{ACI} term is calculated as (Eq. 3):

  $$RE_{ACI} = \Delta\left(F_{af} - F_{csaf}\right) \quad (3)$$

  where F_{af} is the net radiative flux at the TOA calculated ignoring the scattering and absorption by aerosols, despite their presence in the atmosphere (i.e., aerosol-free forcing), F_{csaf} is the corresponding flux calculated neglecting the scattering and absorption by both aerosols and clouds despite their presence in the atmosphere (i.e., clear-sky, aerosols-free forcing), and Δ denotes the difference between the perturbation and the control experiment.

- RE_{res}: The residual term represents the portion of the total radiative effect not attributed to aerosol-radiation or aerosol-cloud interactions and is diagnosed as a remainder of the decomposition. Specifically, RE_{res} includes the radiative impacts associated with changes in atmospheric composition (e.g., O_3), and the feedbacks (e.g., temperature, humidity and surface albedo) (Zelinka et al., 2014, 2023). According to the decomposition of the RE_{res} term presented by Zelinka et al. (2023), the SW component of RE_{res} includes the change in net radiation caused by surface albedo changes, the aerosol-free clear-sky radiative contributions from humidity changes, and a masking term which

https://doi.org/10.5194/egusphere-2026-3239
Preprint. Discussion started: 18 June 2026

represents the radiative impact of surface albedo changes that are attenuated by the presence of both aerosols and clouds. On the other hand, the LW component of RE_{res} includes the aerosol-free clear-sky radiative contributions from changes in temperature and humidity, along with changes in tropospheric O_3. The RE_{res} term is calculated as (Eq. 4):

$$RE_{res} = \Delta F_{csaf} \quad (4)$$

where F_{csaf} is the net radiative flux at TOA calculated neglecting the scattering and absorption by both aerosols and clouds despite their presence in the atmosphere (i.e., clear-sky, aerosols-free forcing), and Δ denotes the difference between the perturbation and the control experiment.

It is noted that in the present work, land surface albedo is determined as (Eq. 5):

$$\frac{Surface\ Upwelling\ Shortwave\ Radiation}{Surface\ Downwelling\ Shortwave\ Radiation} \quad (5)$$

Moreover, due to the of the adopted model configuration, surface radiation is affected by snow cover and snow depth changes, and not by the vegetation cover and background soil albedo changes, since these are prescribed (Döscher et al., 2022; van Noije et al., 2021). In addition, the snow darkening effect of black carbon (BC) deposition is not represented, as the model does not account for it during the radiation calculation.

2.3 Total, fast and slow climate responses

To further investigate the mechanisms behind the climate impacts of wildfire emissions, the total climate response is decomposed into its fast and slow components (Andrews et al., 2010; Liu et al., 2018; Myhre et al., 2017; Samset et al., 2016; Zhang et al., 2021). Specifically, the fast response is diagnosed via the atmosphere-only simulations and represents the immediate atmospheric changes that occur in direct response to wildfire-induced perturbations independently of sea surface temperature (SST) changes, as opposed to the total climate responses, which can be diagnosed via the fully coupled ocean-atmosphere simulations. The definition of the relevant diagnostics adopted in the current study is presented below.

- Temperature Response (K): we diagnose the fast temperature response via the atmosphere-only simulations, while the total temperature response is derived from fully coupled ocean–atmosphere simulations.
- Precipitation Response (mm/day): We separate the precipitation response into fast, slow, and total components as proposed by previous studies (Liu et al., 2018; Myhre et al., 2017; Samset et al., 2016).

  Fast precipitation response: Diagnosed from the atmosphere-only simulations. This component represents rapid adjustments of the hydrological cycle to radiative forcing, occurring independently of global surface temperature change. These adjustments are primarily driven by changes in atmospheric radiative heating and stabilization effects.

  Total precipitation response: Diagnosed from the fully coupled ocean–atmosphere simulations. This response includes both fast adjustments and temperature-mediated (slow) changes.

https://doi.org/10.5194/egusphere-2026-3239
Preprint. Discussion started: 18 June 2026

Slow precipitation response: Calculated as the difference between the total and fast precipitation responses. This component represents precipitation changes that scale with global surface temperature change and are largely controlled by energetic constraints on the hydrological cycle.

Moreover, the Net Atmospheric Absorption (AA) (W/m^2) was determined. AA is defined as the difference between the TOA and surface radiative effects. It represents the net radiative energy absorbed within the atmospheric column. A positive AA indicates increased atmospheric heating, while negative AA indicates decreased heating.

2.4 Wildfire emissions – global and regional analysis

In this section, the CMIP6 wildfire emissions applied (2015 according to the SSP3-7.0 scenario) (Feng et al., 2020) are discussed (Figure 2 and Table S1). The CMIP6 wildfire dataset includes emissions of black carbon (BC), organic carbon (OC), carbon monoxide (CO), methane (CH_4), ammonia (NH_3), sulfur dioxide (SO_2), nitrogen oxides (NO_x), non-methane volatile organic compounds (NMVOCs), and carbon dioxide (CO_2). The radiative effects of CO_2 and CH_4 are not considered here, as their mixing ratios were prescribed to 2015 levels, taking into account their atmospheric lifetimes relative to the simulation period. The focus of this study is on short-lived species: BC, OC, SO_2, NH_3, NMVOCs, NO_x, and CO, which are either aerosols, aerosol precursors, or ozone (O_3) precursors. The primary objective of this work is to investigate the radiative effects of wildfire-emitted aerosols and the secondary formation of O_3.

On a global and annual scale, in terms of total mass, CO is the most abundantly emitted short-lived constituent (approximately 328 Tg), followed by NMVOCs (approximately 63 Tg), OC (approximately 15 Tg), NO_x (approximately 14 Tg), NH_3 (approximately 3.9 Tg), SO_2 (approximately 2.2 Tg) and BC (approximately 1.7 Tg). Africa (AF) is the main source of wildfire emissions, emitting approximately 36% - 62% of the total global emissions depending on the species, followed South America (SA) (13% - 16.5%), Boreal & Central Asia (BCA) (4% - 19%), Equatorial Asia (EQ) (4% - 10.5%), and Boreal North America (BNA) (1% - 9%) (Figure 2 and Table S1).

https://doi.org/10.5194/egusphere-2026-3239
Preprint. Discussion started: 18 June 2026

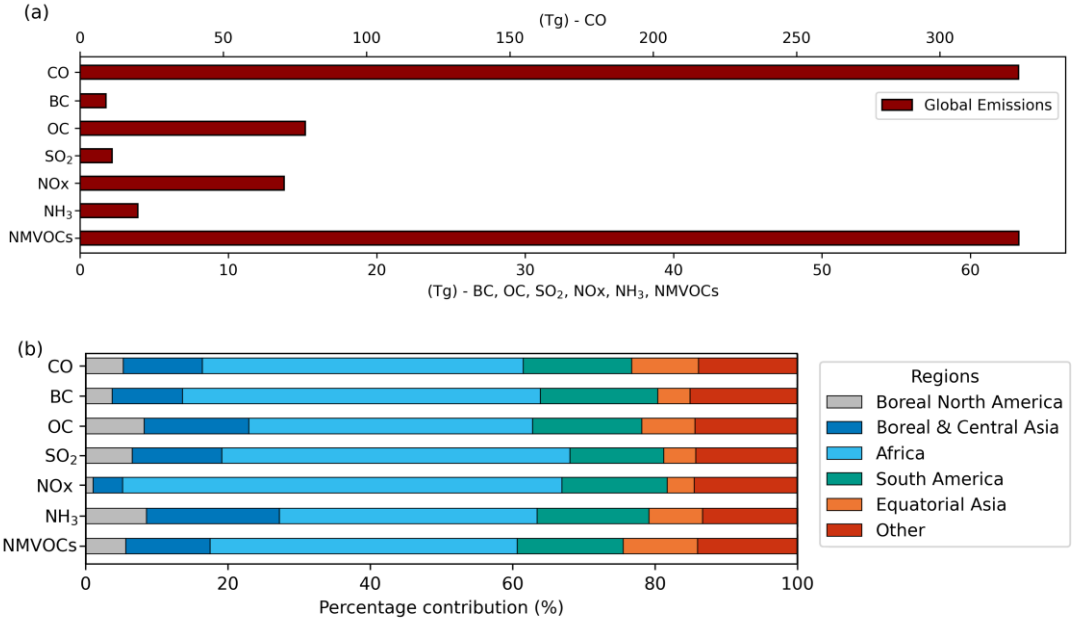

Figure 2: Panel (a) Total global wildfire emissions (in Tg) per species for the year 2015 of the CMIP6 wildfire dataset (scenario SSP3-7.0) (Feng et al., 2020). Panel (b) Regional percentage contribution (%) to the total global wildfire emissions for 2015.

2.5 Post-Processing and Statistical Methods

The ece2cmor3 tool was used for post-processing the EC-Earth3 output (van den Oord and Bakhshi, 2017).

The Welch's t-test (Welch, 1947) was applied to assess the statistical significance of differences between the control and perturbation simulations. The t-statistic was computed as follows (Eq. 6):

$$t = \frac{\overline{X_{PE}} - \overline{X_C}}{\sqrt{SE^2_{\overline{X_{PE}}} + SE^2_{\overline{X_C}}}} \quad (6)$$

Where:

- $\overline{X_{PE}}$ and $\overline{X_C}$ are the means of the perturbation and control simulations, respectively
- $SE_{\overline{X_{PE}}}$ and $SE_{\overline{X_C}}$ are the standard errors of the means, calculated as (Eq. 7):

$$SE_{\overline{X_{PE}}} = \frac{s_{PE}}{\sqrt{n}}, \; SE_{\overline{X_C}} = \frac{s_C}{\sqrt{n}} \quad (7)$$

- s_{PE} and s_C represent the standard deviations for the perturbation and control simulations, respectively, and,
- n is the sample size, which corresponds to 30 for the atmosphere-only simulations, and to 50 for the fully coupled ocean-atmosphere simulations.

https://doi.org/10.5194/egusphere-2026-3239
Preprint. Discussion started: 18 June 2026

3 Results and discussion

3.1 Aerosols and tropospheric O_3

Our simulations show that global wildfire emissions lead to a pronounced and widespread increases in aerosols and tropospheric O_3 (Figures 3a and 3b). Focusing more on the global effects of the emissions from specific regions of interest, namely, BNA, BCA SA, AF, and EQ, these seem to also affect remote areas, away from the source region (Figures S5-S9). However, the magnitude and spatial extent of these impacts depend strongly on both emission quantity and the location of the source. Briefly, the emissions from AF and SA produce the largest increases in aerosol optical depth (AOD) and tropospheric O_3, consistent with their higher emissions magnitudes compared to BNA, BCA, and EQ. Notably, AF emissions cause a pronounced and extensive increase in tropospheric O_3 on a global scale, affecting most regions. This could be attributed both to AF's abundant emissions and to the increased photochemical production of O_3 from precursors in the tropics due to stronger incoming shortwave radiation.

Despite BNA and EQ having comparable emissions, EQ emissions cause a more localized but pronounced increase in AOD, whereas BNA emissions lead to a more widespread yet weaker AOD increase, which could be explained by the corresponding effects of atmospheric circulation (Figure S1). Specifically, EQ emissions appear to be transported mainly toward Southeast Asia (Figure S9), while BNA emissions are dispersed over more remote regions by the polar jet stream and NH westerlies (Figures S1 and S5). This broader dispersion of wildfire emissions leads to a more diluted and therefore less pronounced AOD increase in terms of magnitude, compared to the case of EQ emissions. Regarding tropospheric O_3, EQ emissions cause both more pronounced and more widespread increases than BNA emissions (Figures S5 and S9). Similar to AF, this response could be explained by the higher emissions of O_3 precursors from EQ (Figure 2) by the more favorable photochemical conditions for O_3 production in the tropics. In addition, O_3 has a longer atmospheric lifetime than aerosols, allowing it to persist during transport and spread over larger spatial scales. As a result, EQ emissions seem to lead to a more widespread increase of tropospheric O_3 despite the less favorable conditions for emission transport compared to BNA.

Regarding the mid- and high-latitudes of the Northern Hemisphere (NH), BCA emissions are higher than those from BNA and consequently lead to more pronounced and more widespread increases in both AOD and tropospheric O_3. This is particularly evident in the case of tropospheric O_3, as BCA emissions induce O_3 increases which extend into tropical and subtropical regions, while BNA effects on O_3 seem comparatively weaker. Emission transport in boreal regions is favorable due to the polar jet stream and NH westerlies. However, despite the similar transport conditions for aerosols, the lower wildfire emissions of BNA relative to BCA explains the weaker AOD increase. Regarding tropospheric O_3, the combination of higher O_3 precursor emissions from BCA, efficient long-range transport driven by prevailing wind patterns (Figures S1 and S5-S9), and the relatively longer atmospheric lifetime of O_3 likely explain both the widespread and pronounced increases in the NH, and the O_3 increases in remote tropical and subtropical regions.

https://doi.org/10.5194/egusphere-2026-3239
Preprint. Discussion started: 18 June 2026

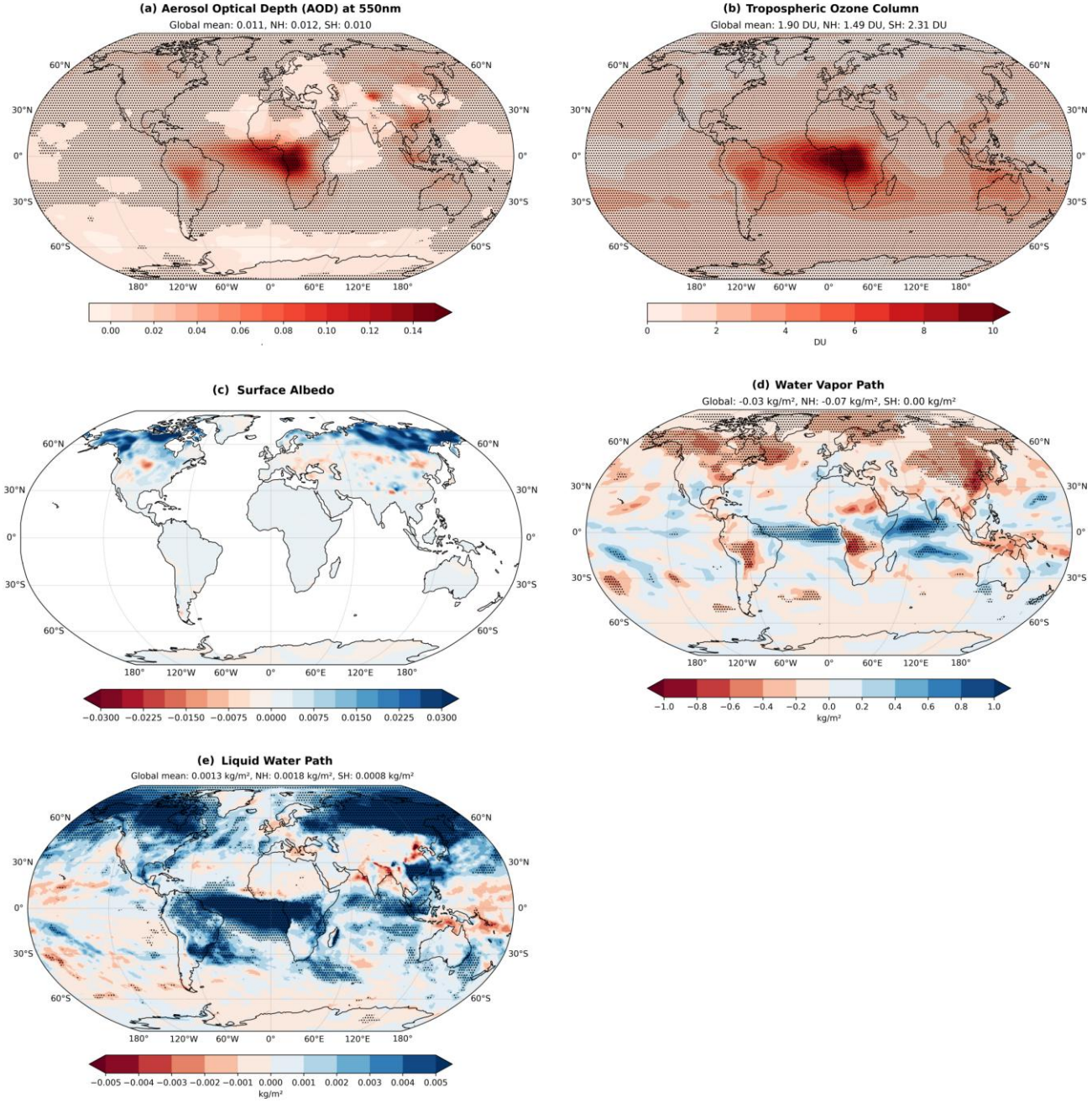

Figure 3: Spatial distribution of the changes in (a) Aerosol Optical Depth (AOD) at 500nm, (b) tropospheric O_3 column (DU), (c) surface albedo, (d) water vapor path (kg/m^2), and (e) liquid water path (kg/m^2) due to the synergistic effect of present-day global wildfire emissions. The maps represent the difference between the 30-year mean of the atmosphere-only perturbation simulations and the 30-year mean of the atmosphere-only control simulations. Black stippling denotes that the change is significant at the 0.05 level.

https://doi.org/10.5194/egusphere-2026-3239
Preprint. Discussion started: 18 June 2026

3.2 Atmosphere-only simulations

3.2.1 Radiative Effect (RE)

When considering the combined effect of all present-day wildfire emissions, they induce a negative RE (cooling effect) on a global scale and in both hemispheres, consistent with the range of reported RE values in the literature (Clark et al., 2015; Grandey et al., 2016; Jiang et al., 2016, 2020; Landry et al., 2017; Tian et al., 2022; Ward et al., 2012; Zou et al., 2020). This negative RE is mainly driven by the changes in downward shortwave radiation, while the changes in downward longwave radiation contribute to the overall forcing direction particularly in the tropics (Table 1, Figure 4). This cooling is dominated by the aerosol–cloud interaction component (RE_{ACI}) (Figure 4b). As already mentioned, wildfire aerosols act as CCN, altering cloud microphysics and often increasing the liquid water content of clouds (represented here as liquid water path, which is the column integral of the liquid water content; Figure 4e), which enhances cloud reflectivity and lifetime. In this work, the spatial distribution of the increases in liquid water path in response to the present-day wildfire emissions coincide with the regions of the pronounced and widespread shortwave cooling associated with RE_{ACI}.

On the contrary, the aerosol–radiation interaction component (RE_{ARI}) (Figure 4c) shows a very small negative value, while the residual term (RE_{res}) (Figure 4d) shows a small positive value (warming effect), partially offsetting the cooling from RE_{ACI}. The spatial distribution of RE (Figure 4a) reveals that the strongest and most widespread effect of the present-day wildfire emissions appears in the mid- and high latitudes of the NH, as well as over Africa (AF), South America (SA), the Atlantic Ocean, Equatorial Asia (EQ), and the Indian Ocean, which is mainly driven by RE_{ACI}. Similar spatial patterns, especially the pronounced negative RE in the NH, were found in previous studies, in which again RE_{ACI} dominates RE (Grandey et al., 2016; Jiang et al., 2016, 2020; Tian et al., 2022; Xu et al., 2021; Zou et al., 2020). Moreover, boreal regions have higher cloud sensitivity to aerosols due to cleaner aerosol background conditions, where even small changes in aerosol concentration can significantly impact cloud properties (Coopman et al., 2018; Koren et al., 2014; Petäjä et al., 2022; Zhao et al., 2025). In tropical regions, however, RE_{ARI} plays a larger role than in the mid- and high latitudes. This is likely reflects the higher incoming shortwave radiation in the tropics, which amplifies the reflection/scattering and absorption of radiation by aerosols. Furthermore, while the higher emissions from AF and SA than in boreal regions may also contribute to stronger RE_{ARI}, EQ emissions are smaller than AF and SA and comparable to BNA (Figure 2), suggesting that the higher incoming shortwave radiation plays a more crucial role in RE than the emissions magnitude alone. It is noted that the positive RE_{ARI} (Figure 4c) over the oceans, such as over Atlantic Ocean, Indian Ocean, and Pacific Ocean, coincide with the positive atmospheric absorption seen in Fig. 4g, indicating the absorbing effect of BC. In addition, RE_{res} emerges as an important contributor in the mid- and high latitudes, where it drives specific regional patterns and contributes to RE. As already mentioned, RE_{res} includes the forcing due to the changes in tropospheric O_3 and the atmospheric feedbacks, such as the changes in water vapor and surface albedo (Figures 3b-3d and Figure 4e). There are widespread increases in tropospheric O_3 and decreases in water vapor at the mid- and high latitudes (Figures 3b and 3d). On the other hand, surface albedo changes have mixed signs in the mid-

https://doi.org/10.5194/egusphere-2026-3239
Preprint. Discussion started: 18 June 2026

latitudes, while mainly increasing in the high-latitudes, where the most widespread and pronounced changes in surface albedo are found (Figure 3c). Unlike surface albedo, water vapor changes are widespread and pronounced across the entire NH and in the low latitudes of the SH (Figure 3b). Although both increases and decreases in water vapor occur in the low latitudes of both hemispheres, the mid- and high latitudes of the NH are characterized mainly by widespread decreases in water vapor. According to Fig. 3 and 4, surface albedo changes seem to qualitatively dominate the RE_{res} term, followed by water vapor and tropospheric O_3. Therefore, considering the aforementioned and the fact that RE_{ACI} dominates the response, even though the secondarily produced tropospheric O_3 shows a widespread and pronounced increase on a global scale, especially in the low latitudes, its effect seems to get overshadowed by the aerosol-induced effects and feedbacks.

Wildfire emissions from the regions of interest (Figures 1 and 2) affect both the source regions and remote areas in terms of radiative effects (Figures S5-S9). The local effects are mainly driven by RE_{ACI}, with RE_{ARI} playing a smaller secondary role. On the other hand, the remote effects are often driven by RE_{res}, with surface albedo changes dominating the mid- and high-latitudes, and water vapor changes drive the RE_{res} term in the low latitudes. Moreover, RE_{ACI} and RE_{ARI} seem to contribute to these remote effects in the low latitudes as well.

To be more specific, BNA emissions cause a negative RE globally and in the NH, but a small positive RE in the SH (Figure S5). Globally, RE_{ACI} is the dominant contributor to RE for BNA emissions, with a pronounced negative value, followed by a smaller negative RE_{res}. These are only minorly offset by a corresponding small positive RE_{ARI}. In the NH, the negative RE is more pronounced and primarily driven by RE_{ACI} with partial offset from positive RE_{ARI} and RE_{res}. In the SH, BNA emissions cause a small positive RE, mainly driven by the RE_{ACI} and partially offset by the small negative RE_{res}. Regarding the spatial distribution of RE, the stronger effect is over BNA and driven by RE_{ACI}.

BCA emissions cause negative RE on a global scale and in the NH, while a positive effect is found for the SH (Figure S6). RE_{ACI} dominates the global and the NH RE, while the positive RE_{ARI} and RE_{res} partially counteract it. In contrast, in the SH, BCA emissions cause positive RE_{ACI}, RE_{ARI} and RE_{res} which jointly contribute to a positive RE. Regarding the spatial distribution of RE, the stronger effect is over BCA and driven by RE_{ACI}.

SA emissions cause a small positive RE globally and a more pronounced positive RE in the NH, while inducing a negative RE in the SH (Figure S7). Globally and in the NH, the negative RE_{ACI} offsets the positive RE_{ARI} and RE_{res}. In the SH, SA emissions cause negative RE_{ACI}, RE_{ARI} and RE_{res} which jointly contribute to a negative RE. Regarding the spatial distribution of RE, the stronger effect is over SA and driven by RE_{ACI}, followed by RE_{ARI}.

Similar to SA, EQ emissions cause a small positive RE on a global scale, a more pronounced positive RE in the NH, and a negative RE in the SH (Figure S9). However, unlike all other regions, the RE caused by the EQ emissions is mainly driven by RE_{ARI}. Globally and in the NH, the positive RE_{ARI} and RE_{res} offset the negative RE_{ACI}. On the other hand, in the SH, RE_{ACI}, RE_{ARI} and RE_{res} have opposite signs, resulting in a negative RE. EQ emissions cause pronounced RE locally, driven by both RE_{ACI} and RE_{ARI}.

AF emissions cause the strongest RE among all regions examined, and are the primary driver of the global wildfire-induced RE (Figure 4 and Figure S8). They cause a pronounced negative RE globally and in both hemispheres, dominated by the RE_{ACI}.

https://doi.org/10.5194/egusphere-2026-3239
Preprint. Discussion started: 18 June 2026

RE_{ARI} contributes to an additional cooling globally and in the NH, but causes a warming effect in the SH, with a small positive value. RE_{res} is positive on a global scale and in both hemispheres, partially offsetting the aforementioned cooling. AF emissions cause a widespread and pronounced negative RE in AF and the Atlantic Ocean, driven by RE_{ACI}.

In the southeast Atlantic region and over AF, RE_{ARI} from AF wildfire emissions exhibits a dipole pattern, with RE_{ARI} being negative over AF and positive over the western coast and the southeast Atlantic (Figure S8). This spatial pattern is also evident in the corresponding maps depicting the combined effect of global wildfire emissions, indicating that it is primarily driven by AF emissions. Previous studies have shown that the overall sign of RE_{ARI} depends strongly on the albedo of the underlying surface beneath absorbing aerosols (Bellouin et al., 2020b; Che et al., 2021; Chen et al., 2024; Giuffrida et al., 2025; Li et al., 2022b). For instance, when BC is above marine clouds or bright land surfaces, such as snow-covered regions or deserts, its RE_{ARI} becomes positive. Clouds and bright surfaces reflect a large portion of the incoming solar radiation upward. Therefore, the BC layer absorbs both the direct incoming solar radiation and the reflected upward radiation, consequently causing positive RE_{ARI}. On the other hand, when absorbing aerosols are above the cloud-free ocean or land with low and variable surface albedo, their RE_{ARI} tends to be either very weak or negative. In contrast, reflective/scattering aerosols, such as OA, are not sensitive to the albedo underneath. In our case, the wildfire-induced change in cloud cover follows the aforementioned dipole pattern in RE_{ARI} (Figure 4c and Figure S2). Over AF, total cloud cover decreases, mainly due to a reduction in high clouds (Figure S2). With fewer high clouds, more incoming solar radiation reaches the wildfire-emitted aerosols, increasing the amount of radiation available for scattering and reflection, enhancing the negative RE_{ARI}. In contrast, over the southeast Atlantic Ocean and along the coast of western AF, both low and high cloud cover increase. On the one hand, the increased high cloud cover reduces the radiation reaching the aerosol layer, and the increased low clouds are below the wildfire-emitted aerosols (Figure S2), leading to more reflections and more radiation for the BC component of the aerosols to absorb. Taken together, they provide a consistent explanation for the positive RE_{ARI} over the southeast Atlantic and the coast of AF. Moreover, our findings are consistent with similar research conducted in the past focusing on the aforementioned region, where wildfire-emitted aerosols caused positive RE_{ARI} over southeast Atlantic and near the coast of AF (Che et al., 2021; Choi and Chung, 2014; Giuffrida et al., 2025).

Similarly to the southeast Atlantic, the northern Atlantic near BNA also experiences positive RE_{ARI} (Figure 4c and Figure S3). However, its signal is less pronounced as both cloud cover and BC increase to a smaller extent than in the southeast Atlantic. The wildfire plume seems to rise above clouds, causing the positive RE_{ARI} (Bellouin et al., 2020b; Che et al., 2021; Chen et al., 2024; Giuffrida et al., 2025). Nevertheless, as in the southeastern Atlantic, the widespread and pronounced negative RE_{ACI} dominates the overall RE, overshadowing the direct effect of absorbing aerosols.

Over the Indian Ocean there is a positive anomaly in the downward longwave radiation associated with the positive RE_{ARI}, despite the negligible increase in AOD (Figure 4c and Figure S4). However, this positive RE_{ARI} coincides with the increased atmospheric absorption (Figure 4g), suggesting that RE_{ARI} in this area is driven by the changes in aerosol loading and the local meteorological effects. First of all, RE_{ARI} over the Indian Ocean can be associated with increased relative humidity, implying increased aerosol water uptake and, consequently, greater longwave absorption by hygroscopic aerosol particles (Figure S4).

https://doi.org/10.5194/egusphere-2026-3239
Preprint. Discussion started: 18 June 2026

Secondly, the RE_{ARI} coincides with increases in the Lagrangian tendency of vertical velocity (ω), indicating enhanced aerosol uplift. Consistent with this interpretation, vertical profiles of organic aerosol (OA) and black carbon (BC) mass mixing ratios suggest modest increases in aerosol concentrations between approximately 700 and 250 hPa relative to lower levels. These increases do not necessarily produce significant AOD anomalies, since AOD represents the integrated aerosol burden across the full atmospheric column. However, uplifted BC aerosols can absorb and re-emit longwave radiation at higher altitudes, where ambient temperatures are lower. Because radiative emission decreases with temperature, this process reduces longwave re-emission to space and increases atmospheric radiative retention, thereby generating a greenhouse-like effect mediated by aerosols. This mechanism appears to be further amplified by substantial reductions in aerosol liquid water content at lower levels within the region of interest. As a result, a larger fraction of upwelling longwave radiation can propagate into the upper troposphere, where absorption by elevated aerosol becomes more effective. Overall, the positive RE_{ARI} over the Indian Ocean appears to be driven from a complex interaction between enhanced aerosol humidification, vertical uplift, and reduced low-level aerosol liquid water content.

Several regions are consistently affected by wildfire emissions originating from remote sources (Figures S5-S9). However, these remote effects are often overshadowed by the RE of local emissions. For example, a region in western BNA exhibits a consistently positive RE induced by BCA, SA, AF, and EQ emissions. This signal is driven by RE_{res} mainly via the surface albedo changes. While a similar positive RE_{res} is also evident as a response to BNA emissions, it is largely masked by the stronger negative RE_{ACI}. Another region showing a consistent remote signal is located in SA, where BNA, BCA, AF, and EQ emissions cause a positive RE driven by RE_{ACI}. However, this signal is overshadowed by the stronger negative RE_{ACI} caused by the local SA wildfire emissions. Asia is also affected by emissions from all the abovementioned regions, exhibiting spatially heterogeneous RE responses. In the mid- and high latitudes, pronounced RE patterns are mainly driven by RE_{res} associated with surface albedo changes, whereas in the low latitudes, RE is driven by RE_{res} due to water vapor changes and RE_{ACI}. Nevertheless, these remote effects are largely offset by the strong RE_{ACI} and RE_{res} caused by the BCA. Finaly, the pronounced negative RE found over the South Pacific Ocean and the Indian Ocean near Australia (Figure 4a and Figures S5-S9) is not directly attributable to the wildfire emissions originating from any of the abovementioned regions under investigation.

https://doi.org/10.5194/egusphere-2026-3239
Preprint. Discussion started: 18 June 2026

Table 1: Global and hemispheric means of RE, RE_{ARI}, RE_{ACI}, and RE_{res}, caused by the global present-day wildfire emissions, as well as from emissions from selected regions, namely Boreal North America (BNA), Boreal & Central Asia (BCA), South America (SA), Africa (AF), and Equatorial Asia (EQ). NH corresponds to the Northern Hemisphere and SH to the Southern Hemisphere.

Wildfire emissions origin	RE (W/m^2)			RE_{ARI} (W/m^2)			RE_{ACI} (W/m^2)			RE_{res} (W/m^2)		
	Global	**NH**	**SH**	**Global**	**NH**	**SH**	**Global**	**NH**	**SH**	**Global**	**NH**	**SH**
Global	-0.71	-0.91	-0.51	-0.00	0.04	-0.04	-0.77	-0.98	-0.55	0.06	0.04	0.09
BNA	-0.12	-0.27	0.04	0.01	0.02	0.00	-0.12	-0.31	0.07	-0.01	0.02	-0.03
BCA	-0.07	-0.27	0.13	0.08	0.09	0.08	-0.17	-0.40	0.05	0.03	0.05	0.00
SA	0.03	0.15	-0.09	0.02	0.06	-0.01	-0.07	-0.08	-0.05	0.08	0.18	-0.02
AF	-0.24	-0.18	-0.30	-0.01	-0.04	0.02	-0.27	-0.18	-0.36	0.05	0.05	0.05
EQ	0.05	0.11	-0.01	0.04	0.08	-0.01	0.00	-0.02	0.01	0.02	0.05	-0.01

https://doi.org/10.5194/egusphere-2026-3239
Preprint. Discussion started: 18 June 2026

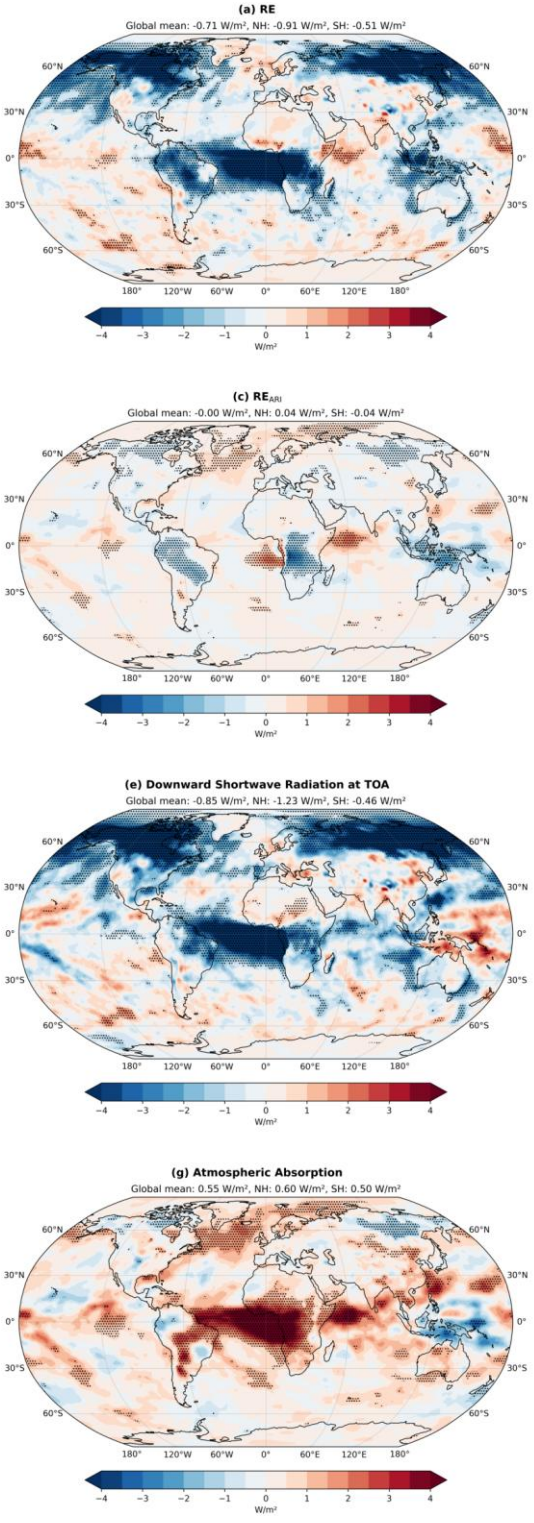

https://doi.org/10.5194/egusphere-2026-3239
Preprint. Discussion started: 18 June 2026

Figure 4: Spatial distribution of (a) the Radiative Effect (RE) (W/m^2) of the present-day global wildfire emissions, and its decomposition into the RE due to (b) the Aerosol-Radiation Interactions (RE$_{ARI}$), (c) the Aerosol-Cloud Interactions (RE$_{ACI}$), and (d) the residual term (RE$_{res}$). Moreover, (e) the shortwave and (f) longwave components of RE are presented, along with (g) the Atmospheric Absorption. The maps represent the difference between the 30-year mean of the atmosphere-only perturbation simulations and the 30-year mean of the control simulations. Black stippling denotes that the change is significant at the 0.05 level.

3.2.2 Fast climate responses

We proceed to analyse the synergistic effects of the global wildfire emissions on climate on short timescales, as well as the individual effects from the different source regions (Figure 1). When it comes to precipitation, the most pronounced changes due to wildfire emissions occur in the low latitudes (fast response; Figure 5). These changes are primarily driven by convection, while the changes in large-scale precipitation seem to play a secondary role (Figure 5 and Figure S10). Nevertheless, the magnitude of total precipitation changes is smaller in the mid and high latitudes compared to the low latitudes. Overall, the spatial patterns of total, convective, and large-scale precipitation fast responses are broadly consistent with previous studies (Grandey et al., 2016; Jiang et al., 2016, 2020; Li et al., 2022a; Tian et al., 2022; Tosca et al., 2013).

Due to the combined effect of global wildfire emissions, the global annual mean precipitation decreases by 0.01 mm/day, while the corresponding reductions on the NH and the SH are 0.01 and 0.02 mm/day, respectively (Table 2 and fast response; Figure 5g-i). The individual effects of wildfire emissions originating from the regions of interest, namely BNA, BCA, SA, AF, and EQ, on precipitation are small when considered at the global scale and across both hemispheres, as reflected in the global and hemispheric mean responses (Table 2). On the other hand, it is worth noting that regional wildfire emissions exert widespread and pronounced impacts on precipitation on the low latitudes independently of the geographic location of the source (Figure S10). For instance, the pronounced precipitation changes over SA, and EQ are the synergistic effect of remote source regions rather than being driven predominantly by local wildfire emissions. An exception is the strong suppression of precipitation over central AF, which is primarily attributable to local wildfire emissions. Moreover, in all cases examined, precipitation changes are correlated with changes in latent heat flux (Figure S12), particularly over land and at low latitudes where convective precipitation dominates, due to the rapid adjustments of the surface.

The global annual mean surface temperature response to the combined effects of global wildfire emissions is small (−0.03 K), indicating a small cooling that is confined to the land (fast response; Figure 6b and Table 2). Similar behavior has been observed in previous studies, in which the fast temperature responses are restricted to the land due to the prescribed SSTs (Jiang et al., 2016, 2020; Kasoar et al., 2018; Liu et al., 2018; Tian et al., 2022; Zhang et al., 2021). In general, the surface temperature feedbacks, are mainly driven by the advection of colder and warmer air masses by atmospheric circulation. For instance, the widespread and pronounced cooling over Boreal and Temperate North America can be attributed to the transport of cold air via the polar jet stream (Figure S1). Similarly, the cooling over AF and SA may result from pole-to-equator cold air transport. Moreover, the warming found in the Arctic is consistent with previous studies (Jiang et al., 2016, 2020; Wu et al., 2024; Zhong

https://doi.org/10.5194/egusphere-2026-3239
Preprint. Discussion started: 18 June 2026

et al., 2024) and appears to be linked to the advection of warmer air from lower latitudes. In contrast, the warming over specific regions of SA, southern AF, and Australia may be associated with the suppression of precipitation in these areas (fast response; Figures 5g-i and 6b).

Similarly to precipitation responses, regional wildfire emissions affect the surface temperature of remote areas (Figure S11); for instance, BNA, SA, AF and EQ wildfire emissions cause a widespread and pronounced warming over northern and central Asia and Europe, which is largely offset by the pronounced cooling induced by the BCA wildfire emissions. In addition, BNA, SA, AF, BCA and EQ wildfire emissions cause warming over southern SA, cooling over eastern central and northern SA, and contribute to the widespread and pronounced cooling over Boreal and Temperate North America. However, AF, SA, and EQ wildfire emissions cause warming in specific regions of Boreal and Temperate North America which is overshadowed by the pronounced cooling caused by the BCA and BNA emissions. Similarly, AF and SA emissions counteract the warming over Africa induced by EQ emissions. Finally, EQ emissions appear to exert stronger surface temperature responses in remote regions than within the source region itself. These fast temperature responses are consistent with the spatial patterns of sensible heat flux changes (Figure S13), which further support the proposed mechanisms. Overall, the wildfire emissions originated from BNA and BCA cause a small cooling on a global scale and in both hemispheres (Table 2), while the wildfire emissions from the SA, AF and EQ cause a small warming, which is driven by the widespread warming of the NH.

Table 2: Global and hemispheric means of the change in Near-Surface Temperature (K) and Total Precipitation (mm/day) as fast responses to the present-day wildfire emissions. This table presents the synergistic effect of the global present-day wildfire emissions, as well as the effects of the selected wildfire emissions region source (Figure 1), namely Boreal North America (BNA), Boreal & Central Asia (BCA), South America (SA), Africa (AF), and Equatorial Asia (EQ). NH corresponds to the Northern Hemisphere and SH to the Southern Hemisphere

Wildfire emissions origin	Near-Surface Temperature (K)			Total Precipitation (mm/day)		
	Global	**NH**	**SH**	**Global**	**NH**	**SH**
Global	-0.03	-0.06	-0.03	-0.012	-0.006	-0.018
BNA	-0.01	-0.01	-0.01	-0.002	0.006	-0.010
BCA	-0.04	-0.06	-0.04	0.000	-0.000	0.001
SA	0.01	0.02	0.01	-0.002	0.009	-0.013
AF	0.00	0.01	0.00	-0.005	-0.004	-0.006
EQ	0.02	0.03	0.02	-0.001	-0.001	-0.000

https://doi.org/10.5194/egusphere-2026-3239
Preprint. Discussion started: 18 June 2026

3.3 Fully coupled ocean-atmosphere simulations

The widespread and pronounced negative RE discussed earlier (Figure 4) induces decreases in the near-surface air temperature (total response; Figure 6a). Global wildfire emissions induce an overall global cooling of approximately -0.51 K, with a stronger effect in the NH (-0.77 K) compared to the SH (-0.25 K). The cooling is larger in the mid and high latitudes and becomes particularly pronounced in the Arctic, where it reaches nearly 2 K. This latitudinal amplification of the cooling is consistent with findings from previous studies focusing on the climate effects of aerosols and Near Term Climate Forcers (NTCFs) emitted from wildfires, anthropogenic activities, or from multiple sources (Jiang et al., 2020; Kasoar et al., 2018; Li, 2020; Li et al., 2022a; Liu et al., 2018; Santos-Espeso et al., 2025; Zhang et al., 2021). In low latitudes, the cooling is more pronounced over land than over ocean. In general, previous studies have attributed this contrast to the lower heat capacity of land compared to oceans (Jiang et al., 2020; Zhang et al., 2021).

Notably, warming is observed over the North Atlantic Warming Hole (NAWH) (SST response; Figure S15, and near-surface temperature total response; Figure 6a) (Li and Liu, 2025). This warming is consistent with previous studies, such as the one conducted by Qasmi (2023), who studied the effects of anthropogenic aerosols. Moreover, Kasoar et al. (2018) and Kusakabe & Takemura (2023) found that the removal of SO_2 emissions produces, on the one hand, a widespread warming, while on the other hand, it causes a cooling anomaly over the NAWH region, a pattern that is effectively inverse of the response to the wildfire emissions of the present work. Therefore, the aforementioned response to the present-day wildfire aerosols suggests that the attenuation of the NAWH is associated with a slight strengthening of the AMOC, given that a weakened AMOC is known to contribute to the development of the NAWH (Li and Liu, 2025). This is confirmed by the pattern of the SST anomaly (Figure S14), which aligns with the longitudinal positioning of the AMOC, including the western warm, shallow upper branch and the eastern cold, deep return branch (McCarthy et al., 2020).

The slow temperature response that drives the total response reflects the oceans' gradual heat release in order to reach the new equilibrium (Ceppi et al., 2018). While the fast temperature response consists of the immediate atmospheric adjustments to the perturbation, it is the slow, ocean-mediated response that is responsible for the aforementioned large-scale cooling dominating the globe, due to the present-day wildfire emissions. In other words, the slow response allows the initial localized fast temperature response to dominate the rest of the hemisphere, via ocean circulation (total response; Figure 6a). Without the ocean's ability to store and move this energy, the temperature response would remain largely confined to the region directly above the forcing.

Global wildfire emissions lead to a suppression of precipitation at the global scale and in both hemispheres when it comes to the total and slow precipitation responses (total and slow responses; Figure 5a-f, and Table 3). It is noted that the slow responses dominate the total precipitation response. Similar to the fast response, the total and slow precipitation changes are most pronounced in the tropics, with particularly strong signals over the North Atlantic and North Pacific Oceans. Convective precipitation dominates the precipitation responses, while large-scale precipitation plays a secondary role. Overall,

https://doi.org/10.5194/egusphere-2026-3239
Preprint. Discussion started: 18 June 2026

precipitation suppression is stronger in the NH than in the SH, except for the large-scale precipitation component, where the opposite pattern is observed.

As shown in Fig. 5 (total and slow response), the precipitation anomalies, particularly over the Pacific Ocean, resemble an amplification of the warming phase of the El Niño–Southern Oscillation (ENSO) (Trenberth et al., 2007), with precipitation shifting from the Maritime Continent to central Pacific, and drying several tropical oceanic regions. This pattern, together with eastward zonal wind anomalies (Figure S1) indicating a weakened Walker circulations, is characteristic of El Niño-like atmospheric conditions (Falster et al., 2023). However, the oceanic response differs: the Niño 3.4 SST anomalies show a decrease in SSTs due to present-day wildfire emissions (Figure S15; mean: -0.31 °C), which is inconsistent with the typical oceanic warming associated with El Niño. In contrast, the Southern Oscillation Index (SOI), which reflects the atmospheric component of ENSO variability, exhibits negative anomalies (Figure S16; mean: -0.20), a pattern generally associated with El Niño conditions. The aforementioned suggests a partial decoupling between the atmospheric and the oceanic ENSO components, as also noted by Bayr et al. (2020) From a dynamical perspective, this behavior implies a disruption of the Bjerknes feedback (Bjerknes, 1969), which links eastern Pacific SST anomalies with atmospheric circulation changes and thermocline adjustments, thereby reinforcing ENSO variability. Weakening this feedback could alter ENSO behavior, leading to reduced intensity or increased variability.

The precipitation response in the mid- and high-latitudes shows a mixture of negative (predominantly) and positive changes. The more widespread suppression of precipitation reflects the thermodynamical response to the aforementioned cooling (Figures 5a-f and 6a). On the other hand, the increased precipitation over the North Atlantic Ocean may be linked to a strengthening of the AMOC, which is associated with the increase in precipitation in previous studies (Bellomo et al., 2021, 2023; Mimi and Alam, 2026). Iversen et al. (2023) and Kusakabe & Takemura (2023) associate the development of the NAWH with reduced precipitation, while Bellomo et al. (2021, 2023) and Mimi and Alam (2026) associate the weakening of AMOC with decreased precipitation in the North Atlantic. Taken together, the aforementioned previous findings point to an AMOC strengthening alongside NAWH attenuation as the key drivers of the increased North Atlantic Ocean precipitation in our results presented here (Figures 5a-f).

https://doi.org/10.5194/egusphere-2026-3239
Preprint. Discussion started: 18 June 2026

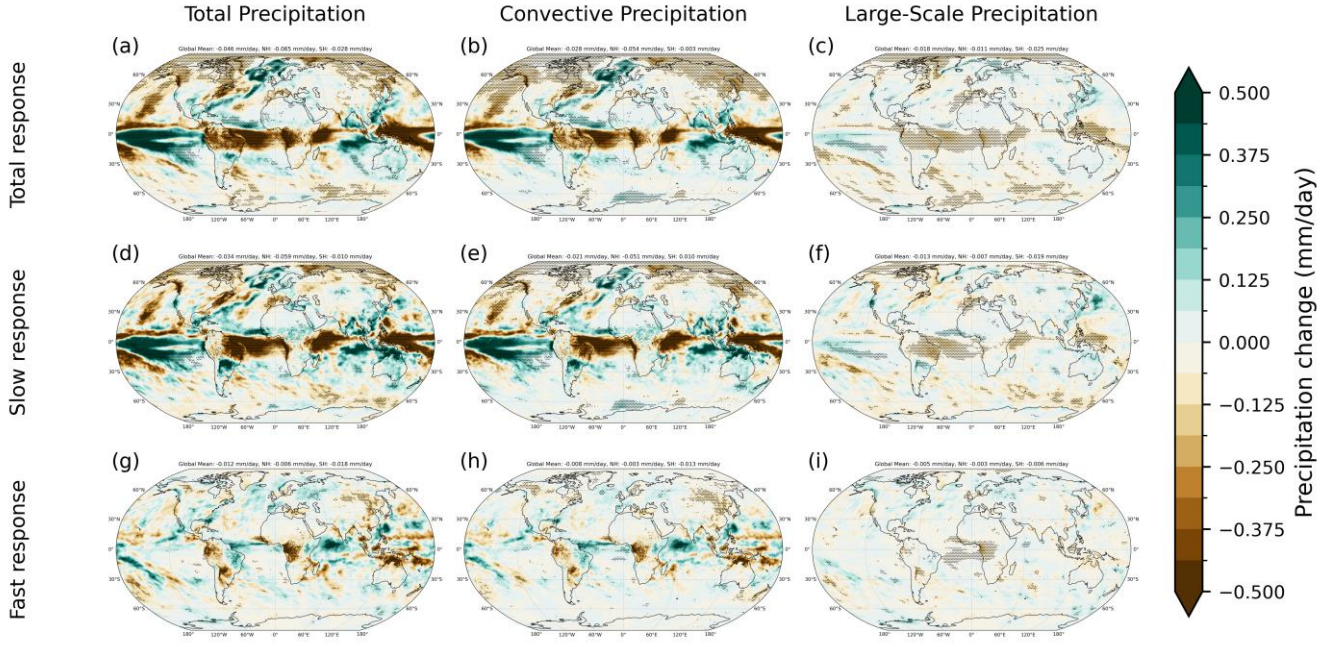

Figure 5: Spatial distribution of the Precipitation Response (mm/day) (total (a)-(c), fast (d)-(f) and slow (g)-(i)) to the present-day global wildfire emissions, and its decomposition into convective and large-scale precipitation. Regarding the fast response, the maps represent the difference between the 30-year mean of the atmosphere-only perturbation simulations and the 30-year mean of the control simulations, while regarding the total response, the difference between the 50-year mean of the fully coupled ocean-atmosphere perturbation simulations and the corresponding control simulations is depicted. Finally, the slow response represents the difference between the total and the fast response. Black stippling denotes that the change is significant at the 0.05 level.

Table 3: Global and hemispheric means of total, convective and large-scale precipitation (mm/day), for the total, slow and fast climate responses to the synergistic effect of present-day wildfire emissions.

	Total Precipitation			Convective Precipitation			Large-Scale Precipitation		
Response	Global	NH	SH	Global	NH	SH	Global	NH	SH
Total	-0.046	-0.065	-0.028	-0.028	-0.054	-0.003	-0.018	-0.011	-0.025
Slow	-0.034	-0.059	-0.010	-0.021	-0.051	0.010	-0.013	-0.007	-0.019
Fast	-0.012	-0.006	-0.018	-0.008	-0.003	-0.013	-0.005	-0.003	-0.006

https://doi.org/10.5194/egusphere-2026-3239
Preprint. Discussion started: 18 June 2026

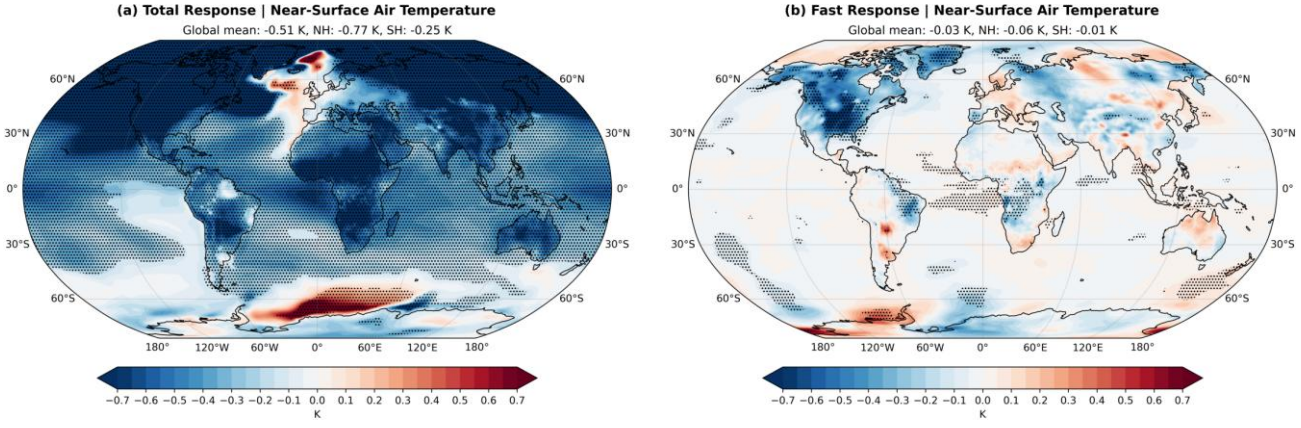

Figure 6: Spatial distribution of the Near-Surface Air Temperature (K) (a) total and (b) fast response to the present-day global wildfire emissions. Regarding the fast response, the maps represent the difference between the 30-year mean of the atmosphere-only perturbation simulations and the 30-year mean of the control simulations, while regarding the total response, the difference between the 50-year mean of the fully coupled ocean-atmosphere perturbation simulations and the corresponding control simulations is depicted. Black stippling denotes that the change is significant at the 0.05 level.

4 Conclusions

Present-day wildfire emissions produce an overall cooling effect (negative Radiative Effect (RE) of approximately -0.71 W/m^2) at the top-of-the-atmosphere (TOA) which is dominated by the aerosol-cloud interactions (RE_{ACI}; approx. -0.77 W/m^2), rather than the direct aerosol-radiation effects (RE_{ARI}; approx. -0.00 W/m^2). RE is mainly driven by the changes in downward shortwave radiation at TOA. However, in the tropics, the changes in downward longwave radiation seem to play an important role in shaping the direction of the RE signal. The atmospheric feedbacks, such as the changes in water vapor and surface albedo, are particularly important in the NH high latitudes, contributing to the total response. The more widespread radiative effects are found on the mid and high-latitudes of the NH, as well as near the tropics in South America, Africa and Atlantic Ocean. The wildfire emissions from Africa (AF), Boreal North America (BNA) and Boreal & Central Asia (BCA) are a main contributor to the global wildfire RE, as they cause widespread and pronounced negative RE (cooling), affecting even remote areas, primarily through strong RE_{ACI}. Equatorial Asia (EQ) is the only region where the aerosol-radiation interactions (RE_{ARI}) dominate the total response. Moreover, the sign and the magnitude of the response are highly dependent on the conditions underlying the wildfire plume and on the aerosol background. Remote effects of emissions are identified, but are typically overshadowed by the impact of regional wildfire emissions. Also, although wildfire emissions substantially increase tropospheric O_3, its warming effect gets overshadowed by the aerosol-driven changes in atmospheric composition and feedbacks. Thus, the aerosol effects dominate the overall response to wildfire emissions. Moreover, our results agree with the reported effect of wildfire-emitted aerosols in the literature; specifically, our RE, RE_{ACI}, and RE_{ARI} are consistent with

https://doi.org/10.5194/egusphere-2026-3239
Preprint. Discussion started: 18 June 2026

previously reported values, and RE_{ACI} is identified as the main driver of RE (Clark et al., 2015; Grandey et al., 2016; Jiang et al., 2016, 2020; Landry et al., 2017; Tian et al., 2022; Ward et al., 2012; Zou et al., 2020).

Regarding the fast climate responses, wildfire emissions can cause large and widespread precipitation changes, especially in the low latitudes, with the global mean indicating a suppression (approximately -0.012 mm/day). Convection is the dominant mechanism of precipitation changes, rather than large-scale phenomena. Overall, the spatial patterns of total, convective, and large-scale precipitation fast responses are broadly consistent with previous studies (Grandey et al., 2016; Jiang et al., 2016, 2020; Li et al., 2022a; Tian et al., 2022; Tosca et al., 2013). Local wildfire emissions are not always the dominant driver of precipitation changes within a region. In several areas, such as South America and Equatorial Asia the largest precipitation anomalies arise from the synergistic effect of remote wildfire source regions rather than local emissions alone. On the other hand, there are some regions, such as Central Africa, where local wildfire emissions are the primary driver of the changes in precipitation patterns. When it comes to fast temperature response, wildfire emissions cause only a small cooling globally (approximately -0.03 K), which agrees with the findings of previous studies (Jiang et al., 2016, 2020; Liu et al., 2018; Tian et al., 2022; Zhang et al., 2021). However, regional surface temperature changes can be more pronounced, especially in the Northern Hemisphere. Moreover, the surface responses are controlled less by local radiative forcing and more by atmospheric circulation and heat transport. Regional wildfire emissions can strongly affect surface temperatures far from their source regions. Overall, the fast precipitation and temperature fast responses show that wildfire impacts are not confined to the source regions. Instead, wildfire emissions alter circulation, land-atmosphere coupling, convection, and energy transport across the globe, producing a highly interconnected climate response.

The slow, ocean-mediated response is the dominant driver of the total climate response on wildfire emissions. Present-day wildfire emissions produce a substantial global cooling (approximately -0.51 K), with stronger cooling in the Northern Hemisphere than in the Southern Hemisphere, as has been demonstrated in the past for aerosols and Near Term Climate Forcers (NTCFs) emitted from wildfires, anthropogenic activities, or from multiple sources (Jiang et al., 2020; Kasoar et al., 2018; Li, 2020; Li et al., 2022a; Liu et al., 2018; Santos-Espeso et al., 2025; Zhang et al., 2021). Total precipitation decreases globally (approximately -0.046 mm/day) and in both hemispheres, with stronger suppression in the Northern Hemisphere. As with temperature, the slow response dominates the total precipitation change, indicating that ocean-driven climate feedbacks are stronger than the immediate atmospheric adjustments. The largest precipitation changes occur in the tropics, especially over the Pacific and Atlantic Oceans. Convective precipitation remains the dominant component of the response, while large-scale precipitation changes are secondary. Overall, the total climate response to wildfire emissions is dominated by slow ocean-atmosphere feedbacks rather than immediate local atmospheric adjustments. These feedbacks amplify the cooling, redistribute it globally, suppress precipitation, and also appear to modify large-scale circulation systems such as the AMOC and ENSO.

Despite the overall agreement of the simulated responses with the literature, some limitations should be considered when interpreting the results. Our analysis relies on a single Earth System Model and a single wildfire emissions dataset. In future work, it would be beneficial to extend these simulations to multi-model intercomparisons and to conduct simulations driven by alternative emission datasets. Such an approach would allow a more systematic assessment of model- and emission-

https://doi.org/10.5194/egusphere-2026-3239
Preprint. Discussion started: 18 June 2026

dependent uncertainties and would help to constrain the robustness of the identified responses across different modelling frameworks and wildfire representations.

However, our results shed light on a relatively unknown forcer of our climate system, i.e., wildfire emissions. They reveal that wildfire emissions are an active component of the climate system, as they can have pronounced effects on climate both locally and in remote areas across the whole globe. Overall, our results demonstrate that present-day wildfire emissions affect climate through complex interactions between aerosols, clouds, atmospheric circulation, and ocean feedbacks, producing substantial regional responses that may exceed what is implied by global mean changes alone.

Code and data availability

The model output used for the present study, as well as the code to produce the figures are publicly available at https://doi.org/10.5281/zenodo.19681847 and https://doi.org/10.5281/zenodo.20043242. For the description and the availability of the forcings and the emissions datasets used in the present work, refer to Döscher et al. (2022) and Feng et al. (2020). Regarding the description of the adopted configuration of EC-Earth3, as well as its availability, refer to Döscher et al. (2022).

Supplement link

The link to the supplement will be included by Copernicus, if applicable.

Author contributions

A.V. conceptualization,; A.V. and R.-N.M. methodology, A.V., R.-N.M. and I.-A.R. validation, R.-N.M. and I.-A.R. formal analysis, R.-N.M. and I.-A.R. investigation, R.-N.M. data curation,; R.-N.M. writing—original draft preparation, A.V., R.-N.M. and I.-A.R. writing—review and editing, R.-N.M. visualization, A.V. supervision, A.V. project administration, A.V funding acquisition.

Competing interests

The authors declare that they have no conflict of interest.

https://doi.org/10.5194/egusphere-2026-3239
Preprint. Discussion started: 18 June 2026

Disclaimer

Copernicus Publications adds a standard disclaimer: "Copernicus Publications remains neutral with regard to jurisdictional claims made in the text, published maps, institutional affiliations, or any other geographical representation in this paper. While Copernicus Publications makes every effort to include appropriate place names, the final responsibility lies with the authors. Views expressed in the text are those of the authors and do not necessarily reflect the views of the publisher."
Please feel free to add disclaimer text at your choice, if applicable.

Acknowledgements

This work was supported by computational time granted from the National Infrastructures for Research and Technology S.A. (GRNET S.A.) in the National HPC facility - ARIS - under project IDs FirePC (pr017) and FirePC2 (pr018).

Financial support

The authors disclose support for the research of this work from the Hellenic Foundation for Research and Innovation (H.F.R.I.) under the project "Fire-emitted Pollution and Climate Change: Linkages in the Past, Present and Future" (grant no. 3453), the Horizon Europe programme under Grant Agreement No 101137680 via project CERTAINTY (Cloud-aERosol inTeractions & their impActs IN The earth sYstem), the AXA Research Fund (project "AXA Chair in Wildfires and Climate", CPO00163217), and the Leverhulme Trust (grant no. RC-2018-023) through the Leverhulme Centre for Wildfires, Environment and Society.

Review statement

The review statement will be added by Copernicus Publications listing the handling editor as well as all contributing referees according to their status anonymous or identified.

References

Albrecht, B. A.: Aerosols, Cloud Microphysics, and Fractional Cloudiness, Science, 245, 1227–1230, https://doi.org/10.1126/science.245.4923.1227, 1989.

Andrews, T., Forster, P. M., Boucher, O., Bellouin, N., and Jones, A.: Precipitation, radiative forcing and global temperature change, Geophys. Res. Lett., 37, https://doi.org/10.1029/2010GL043991, 2010.

https://doi.org/10.5194/egusphere-2026-3239
Preprint. Discussion started: 18 June 2026

Barjeste Vaezi, R., Martin, M. R., and Hosseinpour, F.: Impacts of wildfire smoke aerosols on radiation, clouds, precipitation, climate, and air quality, Atmospheric Environ. X, 26, 100322, https://doi.org/10.1016/j.aeaoa.2025.100322, 2025.

Bayr, T., Dommenget, D., and Latif, M.: Walker circulation controls ENSO atmospheric feedbacks in uncoupled and coupled climate model simulations, Clim. Dyn., 54, 2831–2846, https://doi.org/10.1007/s00382-020-05152-2, 2020.

Bellomo, K., Angeloni, M., Corti, S., and von Hardenberg, J.: Future climate change shaped by inter-model differences in Atlantic meridional overturning circulation response, Nat. Commun., 12, 3659, https://doi.org/10.1038/s41467-021-24015-w, 2021.

Bellomo, K., Meccia, V. L., D'Agostino, R., Fabiano, F., Larson, S. M., von Hardenberg, J., and Corti, S.: Impacts of a weakened AMOC on precipitation over the Euro-Atlantic region in the EC-Earth3 climate model, Clim. Dyn., 61, 3397–3416, https://doi.org/10.1007/s00382-023-06754-2, 2023.

Bellouin, N., Quaas, J., Gryspeerdt, E., Kinne, S., Stier, P., Watson-Parris, D., Boucher, O., Carslaw, K. S., Christensen, M., Daniau, A. -L., Dufresne, J. -L., Feingold, G., Fiedler, S., Forster, P., Gettelman, A., Haywood, J. M., Lohmann, U., Malavelle, F., Mauritsen, T., McCoy, D. T., Myhre, G., Mülmenstädt, J., Neubauer, D., Possner, A., Rugenstein, M., Sato, Y., Schulz, M., Schwartz, S. E., Sourdeval, O., Storelvmo, T., Toll, V., Winker, D., and Stevens, B.: Bounding Global Aerosol Radiative Forcing of Climate Change, Rev. Geophys., 58, https://doi.org/10.1029/2019RG000660, 2020a.

Bellouin, N., Davies, W., Shine, K. P., Quaas, J., Mülmenstädt, J., Forster, P. M., Smith, C., Lee, L., Regayre, L., Brasseur, G., Sudarchikova, N., Bouarar, I., Boucher, O., and Myhre, G.: Radiative forcing of climate change from the Copernicus reanalysis of atmospheric composition, Earth Syst. Sci. Data, 12, 1649–1677, https://doi.org/10.5194/essd-12-1649-2020, 2020b.

Bilbao, R., Wild, S., Ortega, P., Acosta-Navarro, J., Arsouze, T., Bretonnière, P.-A., Caron, L.-P., Castrillo, M., Cruz-García, R., Cvijanovic, I., Doblas-Reyes, F. J., Donat, M., Dutra, E., Echevarría, P., Ho, A.-C., Loosveldt-Tomas, S., Moreno-Chamarro, E., Pérez-Zanon, N., Ramos, A., Ruprich-Robert, Y., Sicardi, V., Tourigny, E., and Vegas-Regidor, J.: Assessment of a full-field initialized decadal climate prediction system with the CMIP6 version of EC-Earth, Earth Syst. Dyn., 12, 173–196, https://doi.org/10.5194/esd-12-173-2021, 2021.

Bjerknes, J.: Atmospheric teleconnections from the equatorial Pacific, Mon. Weather Rev., 97, 163–172, https://doi.org/10.1175/1520-0493(1969)097%3C0163:ATFTEP%3E2.3.CO;2, 1969.

Ceppi, P., Zappa, G., Shepherd, T. G., and Gregory, J. M.: Fast and Slow Components of the Extratropical Atmospheric Circulation Response to CO2 Forcing, J. Clim., 31, 1091–1105, https://doi.org/10.1175/JCLI-D-17-0323.1, 2018.

Chan, C. Y., Chan, L. Y., Zheng, Y. G., Harris, J. M., Oltmans, S. J., and Christopher, S.: Effects of 1997 Indonesian forest fires on tropospheric ozone enhancement, radiative forcing, and temperature change over the Hong Kong region, J. Geophys. Res. Atmospheres, 106, 14875–14885, https://doi.org/10.1029/2001JD900092, 2001.

Chang, D. Y., Yoon, J., Lelieveld, J., Park, S. K., Yum, S. S., Kim, J., and Jeong, S.: Direct radiative forcing of biomass burning aerosols from the extensive Australian wildfires in 2019–2020, Environ. Res. Lett., 16, 044041, https://doi.org/10.1088/1748-9326/abecfe, 2021.

Chaudhary, A., Guntu, R. K., Sharma, S., and Agarwal, A.: Changing spatiotemporal dependence of the precipitation-temperature during Indian Summer Monsoon using observational and CMIP6 model simulations, J. Hydrol. Reg. Stud., 57, 102169, https://doi.org/10.1016/j.ejrh.2024.102169, 2025.

https://doi.org/10.5194/egusphere-2026-3239
Preprint. Discussion started: 18 June 2026

Che, H., Stier, P., Gordon, H., Watson-Parris, D., and Deaconu, L.: Cloud adjustments dominate the overall negative aerosol radiative effects of biomass burning aerosols in UKESM1 climate model simulations over the south-eastern Atlantic, Atmospheric Chem. Phys., 21, 17–33, https://doi.org/10.5194/acp-21-17-2021, 2021.

Chen, A., Zhao, C., Zhang, H., Yang, Y., and Li, J.: Surface albedo regulates aerosol direct climate effect, Nat. Commun., 15, 7816, https://doi.org/10.1038/s41467-024-52255-z, 2024.

Choi, J.-O. and Chung, C. E.: Sensitivity of aerosol direct radiative forcing to aerosol vertical profile, Tellus B Chem. Phys. Meteorol., 66, https://doi.org/10.3402/tellusb.v66.24376, 2014.

Clark, S. K., Ward, D. S., and Mahowald, N. M.: The sensitivity of global climate to the episodicity of fire aerosol emissions, J. Geophys. Res. Atmospheres, 120, 11,589-11,607, https://doi.org/10.1002/2015JD024068, 2015.

Collins, W. J., Lamarque, J.-F., Schulz, M., Boucher, O., Eyring, V., Hegglin, M. I., Maycock, A., Myhre, G., Prather, M., Shindell, D., and Smith, S. J.: AerChemMIP: quantifying the effects of chemistry and aerosols in CMIP6, Geosci. Model Dev., 10, 585–607, https://doi.org/10.5194/gmd-10-585-2017, 2017.

Coopman, Q., Garrett, T. J., Finch, D. P., and Riedi, J.: High Sensitivity of Arctic Liquid Clouds to Long-Range Anthropogenic Aerosol Transport, Geophys. Res. Lett., 45, 372–381, https://doi.org/10.1002/2017GL075795, 2018.

Döscher, R., Acosta, M., Alessandri, A., Anthoni, P., Arsouze, T., Bergman, T., Bernardello, R., Boussetta, S., Caron, L.-P., Carver, G., Castrillo, M., Catalano, F., Cvijanovic, I., Davini, P., Dekker, E., Doblas-Reyes, F. J., Docquier, D., Echevarria, P., Fladrich, U., Fuentes-Franco, R., Gröger, M., v. Hardenberg, J., Hieronymus, J., Karami, M. P., Keskinen, J.-P., Koenigk, T., Makkonen, R., Massonnet, F., Ménégoz, M., Miller, P. A., Moreno-Chamarro, E., Nieradzik, L., van Noije, T., Nolan, P., O'Donnell, D., Ollinaho, P., van den Oord, G., Ortega, P., Prims, O. T., Ramos, A., Reerink, T., Rousset, C., Ruprich-Robert, Y., Le Sager, P., Schmith, T., Schrödner, R., Serva, F., Sicardi, V., Sloth Madsen, M., Smith, B., Tian, T., Tourigny, E., Uotila, P., Vancoppenolle, M., Wang, S., Wårlind, D., Willén, U., Wyser, K., Yang, S., Yepes-Arbós, X., and Zhang, Q.: The EC-Earth3 Earth system model for the Coupled Model Intercomparison Project 6, Geosci. Model Dev., 15, 2973–3020, https://doi.org/10.5194/gmd-15-2973-2022, 2022.

Falster, G., Konecky, B., Coats, S., and Stevenson, S.: Forced changes in the Pacific Walker circulation over the past millennium, Nature, 622, 93–100, https://doi.org/10.1038/s41586-023-06447-0, 2023.

Feng, L., Smith, S. J., Braun, C., Crippa, M., Gidden, M. J., Hoesly, R., Klimont, Z., van Marle, M., van den Berg, M., and van der Werf, G. R.: The generation of gridded emissions data for CMIP6, Geosci. Model Dev., 13, 461–482, https://doi.org/10.5194/gmd-13-461-2020, 2020.

Ghan, S. J.: Technical Note: Estimating aerosol effects on cloud radiative forcing, Atmospheric Chem. Phys., 13, 9971–9974, https://doi.org/10.5194/acp-13-9971-2013, 2013.

Giuffrida, E., Johnson, K., Tatro, T., Zuidema, P., and Gordon, H.: Biomass burning aerosol radiative effects in the Southeast Atlantic depend strongly on meteorological forcing method, Atmospheric Chem. Phys., 25, 14879–14907, https://doi.org/10.5194/acp-25-14879-2025, 2025.

Gliß, J., Mortier, A., Schulz, M., Andrews, E., Balkanski, Y., Bauer, S. E., Benedictow, A. M. K., Bian, H., Checa-Garcia, R., Chin, M., Ginoux, P., Griesfeller, J. J., Heckel, A., Kipling, Z., Kirkevåg, A., Kokkola, H., Laj, P., Le Sager, P., Lund, M. T., Lund Myhre, C., Matsui, H., Myhre, G., Neubauer, D., van Noije, T., North, P., Olivié, D. J. L., Rémy, S., Sogacheva, L., Takemura, T., Tsigaridis, K., and Tsyro, S. G.: AeroCom phase III multi-model evaluation of the aerosol life cycle and optical properties using ground- and space-based remote sensing as well as surface in situ observations, Atmospheric Chem. Phys., 21, 87–128, https://doi.org/10.5194/acp-21-87-2021, 2021.

https://doi.org/10.5194/egusphere-2026-3239
Preprint. Discussion started: 18 June 2026

Grandey, B. S., Lee, H.-H., and Wang, C.: Radiative effects of interannually varying vs. interannually invariant aerosol emissions from fires, Atmospheric Chem. Phys., 16, 14495–14513, https://doi.org/10.5194/acp-16-14495-2016, 2016.

He, C., Kumar, R., Tang, W., Pfister, G., Xu, Y., Qian, Y., and Brasseur, G.: Air Pollution Interactions with Weather and Climate Extremes: Current Knowledge, Gaps, and Future Directions, Curr. Pollut. Rep., 10, 430–442, https://doi.org/10.1007/s40726-024-00296-9, 2024.

Iversen, E. C., Hodnebrog, Ø., Seland Graff, L., Nygaard, B. E., and Iversen, T.: Future Winter Precipitation Decreases Associated With the North Atlantic Warming Hole and Reduced Convection, J. Geophys. Res. Atmospheres, 128, e2022JD038374, https://doi.org/10.1029/2022JD038374, 2023.

Jain, P., Barber, Q. E., Taylor, S. W., Whitman, E., Castellanos Acuna, D., Boulanger, Y., Chavardès, R. D., Chen, J., Englefield, P., Flannigan, M., Girardin, M. P., Hanes, C. C., Little, J., Morrison, K., Skakun, R. S., Thompson, D. K., Wang, X., and Parisien, M.-A.: Drivers and Impacts of the Record-Breaking 2023 Wildfire Season in Canada, Nat. Commun., 15, 6764, https://doi.org/10.1038/s41467-024-51154-7, 2024.

Jiang, Y., Lu, Z., Liu, X., Qian, Y., Zhang, K., Wang, Y., and Yang, X.-Q.: Impacts of global open-fire aerosols on direct radiative, cloud and surface-albedo effects simulated with CAM5, Atmospheric Chem. Phys., 16, 14805–14824, https://doi.org/10.5194/acp-16-14805-2016, 2016.

Jiang, Y., Yang, X.-Q., Liu, X., Qian, Y., Zhang, K., Wang, M., Li, F., Wang, Y., and Lu, Z.: Impacts of Wildfire Aerosols on Global Energy Budget and Climate: The Role of Climate Feedbacks, J. Clim., 33, 3351–3366, https://doi.org/10.1175/JCLI-D-19-0572.1, 2020.

Kalisoras, A., Georgoulias, A. K., Akritidis, D., Allen, R. J., Naik, V., Kuo, C., Szopa, S., Nabat, P., Olivié, D., van Noije, T., Le Sager, P., Neubauer, D., Oshima, N., Mulcahy, J., Horowitz, L. W., and Zanis, P.: Decomposing the effective radiative forcing of anthropogenic aerosols based on CMIP6 Earth system models, Atmospheric Chem. Phys., 24, 7837–7872, https://doi.org/10.5194/acp-24-7837-2024, 2024.

Kasoar, M., Shawki, D., and Voulgarakis, A.: Similar spatial patterns of global climate response to aerosols from different regions, Npj Clim. Atmospheric Sci., 1, 12, https://doi.org/10.1038/s41612-018-0022-z, 2018.

Koren, I., Dagan, G., and Altaratz, O.: From aerosol-limited to invigoration of warm convective clouds, Science, 344, 1143–1146, https://doi.org/10.1126/science.1252595, 2014.

Kramer, R. J., Smith, C., and Andrews, T.: The Radiative Forcing Model Intercomparison Project (RFMIP2.0) for CMIP7, Geosci. Model Dev., 19, 4447–4466, https://doi.org/10.5194/gmd-19-4447-2026, 2026.

Kusakabe, Y. and Takemura, T.: Formation of the North Atlantic Warming Hole by reducing anthropogenic sulphate aerosols, Sci. Rep., 13, 8, https://doi.org/10.1038/s41598-022-27315-3, 2023.

Landry, J.-S., Partanen, A.-I., and Damon Matthews, H.: Carbon cycle and climate effects of forcing from fire-emitted aerosols, Environ. Res. Lett., 12, 025002, https://doi.org/10.1088/1748-9326/aa51de, 2017.

Li, F.: Quantifying the impacts of fire aerosols on global terrestrial ecosystem productivity with the fully-coupled Earth system model CESM, Atmospheric Ocean. Sci. Lett., 13, 330–337, https://doi.org/10.1080/16742834.2020.1740580, 2020.

Li, F., Lawrence, D. M., Jiang, Y., Liu, X., and Lin, Z.: Fire Aerosols Slow Down the Global Water Cycle, J. Clim., 35, 7219–7233, https://doi.org/10.1175/JCLI-D-21-0817.1, 2022a.

https://doi.org/10.5194/egusphere-2026-3239
Preprint. Discussion started: 18 June 2026

Li, J., Carlson, B. E., Yung, Y. L., Lv, D., Hansen, J., Penner, J. E., Liao, H., Ramaswamy, V., Kahn, R. A., Zhang, P., Dubovik, O., Ding, A., Lacis, A. A., Zhang, L., and Dong, Y.: Scattering and absorbing aerosols in the climate system, Nat. Rev. Earth Environ., 3, 363–379, https://doi.org/10.1038/s43017-022-00296-7, 2022b.

Li, K.-Y. and Liu, W.: Weakened Atlantic Meridional Overturning Circulation causes the historical North Atlantic Warming Hole, Commun. Earth Environ., 6, 416, https://doi.org/10.1038/s43247-025-02403-0, 2025.

Liu, L., Shawki, D., Voulgarakis, A., Kasoar, M., Samset, B. H., Myhre, G., Forster, P. M., Hodnebrog, O., Sillmann, J., Aalbergsjo, S. G., Boucher, O., Faluvegi, G., Iversen, T., Kirkevåg, A., Lamarque, J. F., Olivié, D., Richardson, T., Shindell, D., and Takemura, T.: A PDRMIP Multimodel Study on the Impacts of Regional Aerosol Forcings on Global and Regional Precipitation, J. Clim., 31, 4429–4447, https://doi.org/10.1175/JCLI-D-17-0439.1, 2018.

Liu, S., Raghavan, S. V., Ona, B. J., and Nguyen, N. S.: Bias evaluation in rainfall over Southeast Asia in CMIP6 models, J. Hydrol., 621, 129593, https://doi.org/10.1016/j.jhydrol.2023.129593, 2023.

López-Saldaña, G., Bistinas, I., and Pereira, J. M. C.: Global analysis of radiative forcing from fire-induced shortwave albedo change, Biogeosciences, 12, 557–565, https://doi.org/10.5194/bg-12-557-2015, 2015.

McCarthy, G. D., Brown, P. J., Flagg, C. N., Goni, G., Houpert, L., Hughes, C. W., Hummels, R., Inall, M., Jochumsen, K., Larsen, K. M. H., Lherminier, P., Meinen, C. S., Moat, B. I., Rayner, D., Rhein, M., Roessler, A., Schmid, C., and Smeed, D. A.: Sustainable Observations of the AMOC: Methodology and Technology, Rev. Geophys., 58, e2019RG000654, https://doi.org/10.1029/2019RG000654, 2020.

Mimi, M. S. and Alam, M. J.: Impact of the Atlantic Meridional Overturning Circulation on Global Precipitation in CMIP5 Model Projections, Meteorology, 5, 8, https://doi.org/10.3390/meteorology5020008, 2026.

Myhre, G., Shindell, D., Bréon, F.-M., Collins, W., Fuglestvedt, J., Huang, J., Koch, D., Lamarque, J.-F., Lee, D., Mendoza, B., Nakajima, T., Robock, A., Stephens, G., Takemura, T., and Zhang, H.: Anthropogenic and Natural Radiative Forcing, in: Climate Change 2013: The Physical Science Basis. Contribution of Working Group I to the Fifth Assessment Report of the Intergovernmental Panel on Climate Change, edited by: Stocker, T. F., Qin, D., Plattner, G.-K., Tignor, M., Allen, S. K., Boschung, J., Nauels, A., Xia, Y., Bex, V., and Midgley, P. M., Cambridge University Press, Cambridge, United Kingdom and New York, NY, USA, https://doi.org/10.1017/CBO9781107415324.018, 2013.

Myhre, G., Forster, P. M., Samset, B. H., Hodnebrog, Ø., Sillmann, J., Aalbergsjø, S. G., Andrews, T., Boucher, O., Faluvegi, G., Fläschner, D., Iversen, T., Kasoar, M., Kharin, V., Kirkevåg, A., Lamarque, J.-F., Olivié, D., Richardson, T. B., Shindell, D., Shine, K. P., Stjern, C. W., Takemura, T., Voulgarakis, A., and Zwiers, F.: PDRMIP: A Precipitation Driver and Response Model Intercomparison Project—Protocol and Preliminary Results, Bull. Am. Meteorol. Soc., 98, 1185–1198, https://doi.org/10.1175/BAMS-D-16-0019.1, 2017.

Natarajan, M., Pierce, R. B., Schaack, T. K., Lenzen, A. J., Al-Saadi, J. A., Soja, A. J., Charlock, T. P., Rose, F. G., Winker, D. M., and Worden, J. R.: Radiative forcing due to enhancements in tropospheric ozone and carbonaceous aerosols caused by Asian fires during spring 2008, J. Geophys. Res. Atmospheres, 117, https://doi.org/10.1029/2011JD016584, 2012.

van Noije, T. P. C., Le Sager, P., Segers, A. J., van Velthoven, P. F. J., Krol, M. C., Hazeleger, W., Williams, A. G., and Chambers, S. D.: Simulation of tropospheric chemistry and aerosols with the climate model EC-Earth, Geosci. Model Dev., 7, 2435–2475, https://doi.org/10.5194/gmd-7-2435-2014, 2014.

van Noije, T., Bergman, T., Le Sager, P., O'Donnell, D., Makkonen, R., Gonçalves-Ageitos, M., Döscher, R., Fladrich, U., von Hardenberg, J., Keskinen, J.-P., Korhonen, H., Laakso, A., Myriokefalitakis, S., Ollinaho, P., Pérez García-Pando, C., Reerink, T., Schrödner, R., Wyser, K., and Yang, S.: EC-Earth3-AerChem: a global climate model with interactive aerosols

https://doi.org/10.5194/egusphere-2026-3239
Preprint. Discussion started: 18 June 2026

and atmospheric chemistry participating in CMIP6, Geosci. Model Dev., 14, 5637–5668, https://doi.org/10.5194/gmd-14-5637-2021, 2021.

van den Oord, G. and Bakhshi, R.: Parallel Post-Processing of the Earth Climate Model Output, Procedia Comput. Sci., 108, 2473–2477, https://doi.org/10.1016/j.procs.2017.05.146, 2017.

Pan, X., Ichoku, C., Chin, M., Bian, H., Darmenov, A., Colarco, P., Ellison, L., Kucsera, T., da Silva, A., Wang, J., Oda, T., and Cui, G.: Six global biomass burning emission datasets: intercomparison and application in one global aerosol model, Atmospheric Chem. Phys., 20, 969–994, https://doi.org/10.5194/acp-20-969-2020, 2020.

Parrington, M., Whaley, C. H., French, N. H. F., Buchholz, R. R., Pan, X., Wiedinmyer, C., Hyer, E. J., Kondragunta, S., Kaiser, J. W., Di Tomaso, E., van der Werf, G. R., Sofiev, M., Barsanti, K. C., da Silva, A. M., Darmenov, A. S., Tang, W., Griffin, D., Desservettaz, M., Carter, T. (Tess), Paton-Walsh, C., Liu, T., Uppstu, A., and Palamarchuk, J.: Biomass burning emission estimation in the MODIS era: State-of-the-art and future directions, Elem. Sci. Anthr., 13, 00089, https://doi.org/10.1525/elementa.2024.00089, 2025.

Petäjä, T., Tabakova, K., Manninen, A., Ezhova, E., O'Connor, E., Moisseev, D., Sinclair, V. A., Backman, J., Levula, J., Luoma, K., Virkkula, A., Paramonov, M., Räty, M., Äijälä, M., Heikkinen, L., Ehn, M., Sipilä, M., Yli-Juuti, T., Virtanen, A., Ritsche, M., Hickmon, N., Pulik, G., Rosenfeld, D., Worsnop, D. R., Bäck, J., Kulmala, M., and Kerminen, V.-M.: Influence of biogenic emissions from boreal forests on aerosol–cloud interactions, Nat. Geosci., 15, 42–47, https://doi.org/10.1038/s41561-021-00876-0, 2022.

Pincus, R., Forster, P. M., and Stevens, B.: The Radiative Forcing Model Intercomparison Project (RFMIP): experimental protocol for CMIP6, Geosci. Model Dev., 9, 3447–3460, https://doi.org/10.5194/gmd-9-3447-2016, 2016.

Qasmi, S.: Past and future response of the North Atlantic warming hole to anthropogenic forcing, Earth Syst. Dyn., 14, 685–695, https://doi.org/10.5194/esd-14-685-2023, 2023.

Roșu, I.-A., Mourgela, R.-N., Kasoar, M., Boleti, E., Parrington, M., and Voulgarakis, A.: Large-scale impacts of the 2023 Canadian wildfires on the Northern Hemisphere atmosphere, Npj Clean Air, 1, 22, https://doi.org/10.1038/s44407-025-00022-9, 2025.

Roșu, I.-A., Mourgela, R.-N., Kasoar, M., Petrakis, M. P., and Voulgarakis, A.: Severe rapid indian monsoon weakening due to emissions from extreme Canadian wildfires, Npj Nat. Hazards, 3, 19, https://doi.org/10.1038/s44304-026-00184-w, 2026.

Rowlinson, M. J., Rap, A., Hamilton, D. S., Pope, R. J., Hantson, S., Arnold, S. R., Kaplan, J. O., Arneth, A., Chipperfield, M. P., Forster, P. M., and Nieradzik, L.: Tropospheric ozone radiative forcing uncertainty due to pre-industrial fire and biogenic emissions, Atmospheric Chem. Phys., 20, 10937–10951, https://doi.org/10.5194/acp-20-10937-2020, 2020.

Samset, B. H., Myhre, G., Forster, P. M., Hodnebrog, Ø., Andrews, T., Faluvegi, G., Fläschner, D., Kasoar, M., Kharin, V., Kirkevåg, A., Lamarque, J. -F., Olivié, D., Richardson, T., Shindell, D., Shine, K. P., Takemura, T., and Voulgarakis, A.: Fast and slow precipitation responses to individual climate forcers: A PDRMIP multimodel study, Geophys. Res. Lett., 43, 2782–2791, https://doi.org/10.1002/2016GL068064, 2016.

Santos-Espeso, A., Gonçalves Ageitos, M., Ortega, P., Pérez García-Pando, C., Donat, M. G., Samso Cabré, M., and Loosveldt Tomas, S.: Regional climate imprints of recent historical changes in anthropogenic Near Term Climate Forcers, Earth Syst. Dyn., 16, 2161–2186, https://doi.org/10.5194/esd-16-2161-2025, 2025.

https://doi.org/10.5194/egusphere-2026-3239
Preprint. Discussion started: 18 June 2026

Shawki, D., Voulgarakis, A., Chakraborty, A., Kasoar, M., and Srinivasan, J.: The South Asian Monsoon Response to Remote Aerosols: Global and Regional Mechanisms, J. Geophys. Res. Atmospheres, 123, 11,585-11,601, https://doi.org/10.1029/2018JD028623, 2018.

Stocker, M., Ladstädter, F., and Steiner, A. K.: Observing the climate impact of large wildfires on stratospheric temperature, Sci. Rep., 11, 22994, https://doi.org/10.1038/s41598-021-02335-7, 2021.

Tang, B., Hu, W., and Duan, A.: Assessment of Extreme Precipitation Indices over Indochina and South China in CMIP6 Models, J. Clim., 34, 7507–7524, https://doi.org/10.1175/JCLI-D-20-0948.1, 2021.

Thomas, M. A., Wyser, K., Wang, S., Chatziparaschos, M., Georgakaki, P., Costa-Surós, M., Gonçalves Ageitos, M., Kanakidou, M., García-Pando, C. P., Nenes, A., van Noije, T., Le Sager, P., and Devasthale, A.: Recent improvements and maximum covariance analysis of aerosol and cloud properties in the EC-Earth3-AerChem model, Geosci. Model Dev., 17, 6903–6927, https://doi.org/10.5194/gmd-17-6903-2024, 2024.

Thornhill, G. D., Ryder, C. L., Highwood, E. J., Shaffrey, L. C., and Johnson, B. T.: The effect of South American biomass burning aerosol emissions on the regional climate, Atmospheric Chem. Phys., 18, 5321–5342, https://doi.org/10.5194/acp-18-5321-2018, 2018.

Tian, C., Yue, X., Zhu, J., Liao, H., Yang, Y., Lei, Y., Zhou, X., Zhou, H., Ma, Y., and Cao, Y.: Fire–climate interactions through the aerosol radiative effect in a global chemistry–climate–vegetation model, Atmospheric Chem. Phys., 22, 12353–12366, https://doi.org/10.5194/acp-22-12353-2022, 2022.

Tosca, M. G., Randerson, J. T., and Zender, C. S.: Global impact of smoke aerosols from landscape fires on climate and the Hadley circulation, Atmospheric Chem. Phys., 13, 5227–5241, https://doi.org/10.5194/acp-13-5227-2013, 2013.

Trenberth, K. E., Jones, P. D., Ambenje, P., Bojariu, R., Easterling, D., Tank, A. K., Parker, D., Renwick, J. A., Rusticucci, M., Soden, B., and Zhai, P.: Observations: Surface and Atmospheric Climate Change, in: Climate Change 2007: The Physical Science Basis. Contribution of Working Group I to the Fourth Assessment Report of the Intergovernmental Panel on Climate Change, Cambridge University Press, Cambridge, United Kingdom and New York, NY, USA, 2007.

Turnock, S. T., Allen, R. J., Andrews, M., Bauer, S. E., Deushi, M., Emmons, L., Good, P., Horowitz, L., John, J. G., Michou, M., Nabat, P., Naik, V., Neubauer, D., O'Connor, F. M., Olivié, D., Oshima, N., Schulz, M., Sellar, A., Shim, S., Takemura, T., Tilmes, S., Tsigaridis, K., Wu, T., and Zhang, J.: Historical and future changes in air pollutants from CMIP6 models, Atmospheric Chem. Phys., 20, 14547–14579, https://doi.org/10.5194/acp-20-14547-2020, 2020.

Twomey, S.: The Influence of Pollution on the Shortwave Albedo of Clouds, J. Atmospheric Sci., 34, 1149–1152, https://doi.org/10.1175/1520-0469(1977)034%3C1149:TIOPOT%3E2.0.CO;2, 1977.

Vescovini, T., Nabat, P., Mallet, M., and Solmon, F.: Aerosol Direct Radiative Effects From Extreme Fire Events in Australia, California and Siberia Occurring in 2019–2020, J. Geophys. Res. Atmospheres, 129, e2024JD041002, https://doi.org/10.1029/2024JD041002, 2024.

Voulgarakis, A. and Field, R. D.: Fire Influences on Atmospheric Composition, Air Quality and Climate, Curr. Pollut. Rep., 1, 70–81, https://doi.org/10.1007/s40726-015-0007-z, 2015.

Voulgarakis, A., Marlier, M. E., Faluvegi, G., Shindell, D. T., Tsigaridis, K., and Mangeon, S.: Interannual variability of tropospheric trace gases and aerosols: The role of biomass burning emissions, J. Geophys. Res. Atmospheres, 120, 7157–7173, https://doi.org/10.1002/2014JD022926, 2015.

https://doi.org/10.5194/egusphere-2026-3239
Preprint. Discussion started: 18 June 2026

Ward, D. S., Kloster, S., Mahowald, N. M., Rogers, B. M., Randerson, J. T., and Hess, P. G.: The changing radiative forcing of fires: global model estimates for past, present and future, Atmospheric Chem. Phys., 12, 10857–10886, https://doi.org/10.5194/acp-12-10857-2012, 2012.

Welch, B. L.: The Generalization of 'Student's' Problem When Several Different Population Variances Are Involved, Biometrika, 34, 28–35, https://doi.org/10.1093/biomet/34.1-2.28, 1947.

Wells, C. D., Kasoar, M., Bellouin, N., and Voulgarakis, A.: Local and remote climate impacts of future African aerosol emissions, Atmospheric Chem. Phys., 23, 3575–3593, https://doi.org/10.5194/acp-23-3575-2023, 2023.

van der Werf, G. R., Randerson, J. T., Giglio, L., Collatz, G. J., Mu, M., Kasibhatla, P. S., Morton, D. C., DeFries, R. S., Jin, Y., and van Leeuwen, T. T.: Global fire emissions and the contribution of deforestation, savanna, forest, agricultural, and peat fires (1997–2009), Atmospheric Chem. Phys., 10, 11707–11735, https://doi.org/10.5194/acp-10-11707-2010, 2010.

Wu, Y.-T., Liang, Y.-C., Previdi, M., Polvani, L. M., England, M. R., Sigmond, M., and Lo, M.-H.: Stronger Arctic amplification from anthropogenic aerosols than from greenhouse gases, Npj Clim. Atmospheric Sci., 7, 142, https://doi.org/10.1038/s41612-024-00696-0, 2024.

Xu, L., Zhu, Q., Riley, W. J., Chen, Y., Wang, H., Ma, P.-L., and Randerson, J. T.: The Influence of Fire Aerosols on Surface Climate and Gross Primary Production in the Energy Exascale Earth System Model (E3SM), J. Clim., 34, 7219–7238, https://doi.org/10.1175/JCLI-D-21-0193.1, 2021.

Yan, H., Zhu, Z., Wang, B., Zhang, K., Luo, J., Qian, Y., and Jiang, Y.: Tropical African wildfire aerosols trigger teleconnections over mid-to-high latitudes of Northern Hemisphere in January, Environ. Res. Lett., 16, 034025, https://doi.org/10.1088/1748-9326/abe433, 2021.

Zelinka, M. D., Andrews, T., Forster, P. M., and Taylor, K. E.: Quantifying components of aerosol-cloud-radiation interactions in climate models, J. Geophys. Res. Atmospheres, 119, 7599–7615, https://doi.org/10.1002/2014JD021710, 2014.

Zelinka, M. D., Smith, C. J., Qin, Y., and Taylor, K. E.: Comparison of methods to estimate aerosol effective radiative forcings in climate models, Atmospheric Chem. Phys., 23, 8879–8898, https://doi.org/10.5194/acp-23-8879-2023, 2023.

Zhang, S., Stier, P., and Watson-Parris, D.: On the contribution of fast and slow responses to precipitation changes caused by aerosol perturbations, Atmospheric Chem. Phys., 21, 10179–10197, https://doi.org/10.5194/acp-21-10179-2021, 2021.

Zhao, J., Ma, X., Quaas, J., and Yang, T.: How meteorological conditions influence aerosol-cloud interactions under different pollution regimes, Atmospheric Chem. Phys., 25, 17701–17723, https://doi.org/10.5194/acp-25-17701-2025, 2025.

Zhong, Q., Schutgens, N., Veraverbeke, S., and van der Werf, G. R.: Increasing aerosol emissions from boreal biomass burning exacerbate Arctic warming, Nat. Clim. Change, 14, 1275–1281, https://doi.org/10.1038/s41558-024-02176-y, 2024.

Zhu, X., Tang, J., and Yang, Y.: Assessment and Projection of Compound Wind and Precipitation Extremes in EC-Earth3 of CMIP6 Simulations, Asia-Pac. J. Atmospheric Sci., 60, 81–93, https://doi.org/10.1007/s13143-023-00337-1, 2024.

Zou, Y., Wang, Y., Qian, Y., Tian, H., Yang, J., and Alvarado, E.: Using CESM-RESFire to understand climate–fire–ecosystem interactions and the implications for decadal climate variability, Atmospheric Chem. Phys., 20, 995–1020, https://doi.org/10.5194/acp-20-995-2020, 2020.